

Mass Transfer Resistance of CuCl_2 Hydrolysis in a Fixed Bed Reactor

by

Dilum Madushanka Perera Kankanamalage

A Thesis submitted to the School of Graduate Studies in partial fulfillment of the
requirements for the degree of

Master of Engineering

in

Faculty of Engineering and Applied Science, Mechanical Engineering

Memorial University of Newfoundland

October 2023

Abstract

The hydrolysis reaction of the Copper-Chlorine (Cu-Cl) cycle is examined in this research to investigate corresponding reaction kinetics with respect to mass transfer resistance through an experimental approach. The experiment was operated at a temperature of 390 °C at atmospheric pressure. The reaction is heterogeneous in which solid reactant CuCl_2 and gaseous reactant H_2O produce Cu_2OCl_2 and HCl . The heterogeneous behaviour of the reaction causes resistance to mass transfer of gaseous reactant H_2O . The resistance in internal diffusion and a surface reaction with mass transfer were analyzed with respect to the initial solid reactant particle size using a shrinking core model (SCM). The results present the thermophysical property of the reaction rate coefficient 0.20165 s^{-1} for a particle size of $620 \mu\text{m}$ and sphericity of 0.68. The experimentally determined reaction and conversion rates of hydrolysis with respect to time are presented, which are experimentally calculated parameters. Scanning Electron Microscopy (SEM) and X-Ray Diffraction (XRD) analysis were used for more accurate results. An uncertainty analysis for the sensors and transducers of the experiment shows that the experimental results have an uncertainty of $\pm 30.1\%$.

Acknowledgments

My supervisors, Dr. Kevin Pope, Dr. Greg Naterer, and Dr. Kelly Hawboldt, are thanked for their guidance and patience throughout the research thesis to accomplish the objectives. The assistance and financial support from Memorial University of Newfoundland (MUN), Natural Sciences and Engineering Research Council of Canada (NSERC), and Canadian Nuclear Laboratories (CNL) are gratefully acknowledged. The support from Sangali Tindi, Dan McLean, Huda Radwan and my research team is thankfully acknowledged.

Table of Contents

Abstract	i
Acknowledgments	ii
Table of Contents	iv
List of Figures	vi
List of Tables	vii
List of Abbreviations	viii
List of Notations	ix
1 Introduction	1
1.1 Objectives and Expected Contributions of the Research	4
1.2 Overview of the Thesis	5
2 Literature Review	7
2.1 Hydrogen production by thermochemical cycles	7
2.2 Cu-Cl Thermochemical Cycle	10
2.3 Reaction Kinetics	16
2.3.1 Parallel Reactions	16
2.3.2 Pressure Drop of Packed Bed	17
2.3.3 Energy and Exergy Analysis	18
2.3.4 Limiting Thermodynamic Efficiencies of Thermochemical Cycles	18
2.4 Experiments and Results	18
3 Hydrolysis Formulation	24
3.1 Hydrolysis Reaction	24
3.2 Progressive Core Model	24

3.3	Shrinking Core Model	25
3.4	External Diffusion Resistance	25
3.5	Internal Diffusion Resistance	26
3.6	Surface Reaction Resistance	27
3.7	Reaction Kinetics of Hydrolysis Reaction	27
4	Experimental Design	32
4.1	Material Selection for the Apparatus	32
4.2	Reactor and Reactor Bed Design	33
4.3	Pressure Drop of the Experimental Setup	34
4.4	Minimum Fluidization Velocity	37
4.5	Safety and Risk Assessment	38
4.6	Temperature Controller and Electrical Design	39
5	Experimental Measurements	41
5.1	DAQ System	41
5.2	Calculation of Chloride Ions and pH Value	42
5.3	Uncertainty Analysis	45
6	Results and Discussion	47
6.1	Analysis of Reactor Outputs	47
6.2	Partial Pressure and Molar Fraction of Steam	48
6.3	Order of Irreversible Hydrolysis Reaction	48
6.4	Thermophysical Properties	49
6.5	Controlling Resistance	51
6.6	Reaction Rate of Hydrolysis Reaction	52
7	Conclusions and Recommendations	54
7.1	Conclusions	54
7.2	Recommendations	55
	Bibliography	58
	Appendix A - Hydrolysis Reactor Safety Manual	63

List of Figures

1.1	Schematic of the operation of Copper Chlorine cycle	2
1.2	Variation of the cupric chloride conversion time with particle diameter	3
2.1	Powder XRD patterns of the hydrolysis product samples isolated after (a) 15, (b) 30, (c) 45, and (d) 60 min over	8
2.2	Schematic representation of the Copper Chlorine (Cu-Cl) cycle	11
2.3	Oxygen generation by decomposition of Cu_2OCl_2 at 490°C and 1.003 bar	17
2.4	Predicted yield of Cu_2OCl_2 as a function of the $\text{H}_2\text{O} / \text{Cu}$ molar ratio at pressures of 0.5 and 1 bar	20
3.1	Solid reactant particle modelled in a progressive core model	25
3.2	Solid reactant particle modelled in a shrinking core model	26
4.1	Schematic of the experimental design	33
4.2	Hydrolysis reactor design	34
4.3	Design and fabrication of the reactor bed	35
4.4	SEM images of solid reactant CuCl_2	37
4.5	Electrical circuit of the experiment	40
5.1	Completed experimental setup	42
5.2	Process flow diagram of the experiment	43
6.1	Solid samples of reactants and products	48
6.2	Partial pressure and molar fraction of steam over time	49
6.3	Order of hydrolysis reaction	50
6.4	Conversion of hydrolysis reaction over time	50
6.5	Density of H_2O vs. reactor temperature	51

6.6	Time ratio of hydrolysis reaction vs. conversion	52
6.7	CuCl_2 hydrolysis reaction rate over time	52

List of Tables

2.1	Performance comparison of thermochemical cycles	14
2.2	Standard thermophysical properties of CuCl Cycle-related compounds	22
4.1	Corrosive resistance of materials	34
4.2	Parameters of experiments	36
4.3	Pressure drop for component losses	37
4.4	Compound flow rates at the exit of the scrubber	39
5.1	Sensors and transducers used for the experiment	42
5.2	Bias and precision errors associated with the measurement devices	46
5.3	Propagation of experimental uncertainty	46

List of Abbreviations

Ce-Cl Cesium Chlorine

Cu-Cl Copper Chlorine

CuSO₄ Copper Sulphate

EXAFS Extended X-ray Absorption Fine Structure

Fe-Cl Ferrous Chlorine

HTGR High Temperature Gas Reactor

Mg-I Magnesium Iodine

SCWR Super Critical Water Reactor

S/Cu Steam to Copper

SEM Scanning Electron Microscopy

S-I Sulphur Iodide

TG-MS Thermo Gravimetry - Mass Spectrometry

V-Cl Vanadium Chlorine

XRD X-Ray Diffraction

List of Notations

Greek Symbols

Δ	Change
μ	Dynamic viscosity
ξ	Steam to copper ratio
ρ	Density
τ	Time for complete conversion
ϵ	Voidage
ϕ	Sphericity

Alphabetical Symbols

A	Cross sectional area
C	Concentration
d	Diameter of the particle
D	Internal diffusion coefficient
f	Fugacity
g	Gravitational acceleration
H	Height of the scrubber column, Height of packed bed
K	Equilibrium constant of the reversible reaction
k	External diffusion coefficient, Reaction rate coefficient
M	Molecular weight
N	Number of moles
\dot{n}	Molar rate
p	Pressure

pH	Potential of hydrogen value
R	Universal gas constant
Re	Reynolds number
RH	Relative humidity
\dot{r}	Reaction rate
Sc	Schmidt number
T	Temperature
t	Time
u	Velocity of gas
V	Volume of the scrubber
\dot{V}	Volumetric flow rate
X	Reaction extent
y	Mole fraction, Time fraction

Subscripts

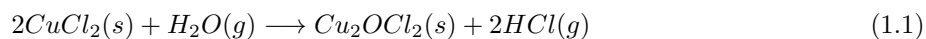
1	Respective to reversible reaction
2	Respective to first order reaction
d	Due to internal diffusion
e	At equilibrium
eff	Effective
g	Gaseous
H	Humidity sensor
i	i-th component
p	Particle
r	Due to surface reaction
sat	Saturated

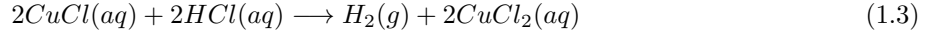
Chapter 1

Introduction

Hydrogen is a promising alternative for a cleaner energy future. The devices and systems used to work on petroleum fuels can be converted to work with hydrogen with nominal modifications. Because of related economic and environmental benefits, clean hydrogen production has been a significant research target. There are various methods to produce hydrogen, such as hydrocarbon oxidation, electrolysis, and water splitting by thermochemical cycles [1,2]. The latter two methods use water as the input for water splitting. To split water directly by thermal energy, high-grade energy, usually through electricity, must be supplied at high temperatures. Therefore, the approach of thermochemical cycles is being analyzed to perform water splitting using low-grade energy as waste heat from power plants at lower temperatures [3,4].

There are more than 200 conceptual thermochemical cycles available in the literature. Nevertheless, less than ten cycles were found to be practically feasible. The Cu-Cl thermochemical cycle became one of the leading cycles due to its advantage of operating in low-temperature requirements (530 °C) over the other cycles. H₂O is used as the input, while hydrogen and oxygen are obtained as the products. The non-consuming Copper(II) chloride and its related compounds ease the production through hydrolysis, thermolysis, electrolysis, drying, and crystallization. The hydrolysis, thermolysis, and electrolysis reactions are demonstrated in equations 1.1, 1.2, and 1.3, respectively. The main types of the Cu-Cl thermochemical cycle are divided into a three-step cycle, four-step cycle, and five-step cycle, according to the number of reactions occurring inside the cycle [1–6].





During the hydrolysis reaction, H_2O vapour reacts with CuCl_2 to make HCl and Cu_2OCl_2 . The reaction is endothermic. Both reactants and products consist of gases and solids. For maximum reaction extent, the temperature has to be maintained between 375 - 400 °C. Thereafter, the product of the hydrolysis reaction, Cu_2OCl_2 , is heated up to 530 °C, becoming the thermolysis reaction. The desired products are O_2 and CuCl . The product O_2 is extracted from the cycle during the thermolysis process. The remaining product, CuCl , reacts with HCl , a hydrolysis reaction product. This is the electrolysis reaction. The respective products are H_2 and CuCl_2 . H_2 is the remaining desired outcome of the thermochemical cycle. The CuCl_2 will be used to react in the hydrolysis reaction again. Therefore, CuCl_2 or its variations are not consumed within the cycle resulting in a sustainable thermochemical cycle [7–9].

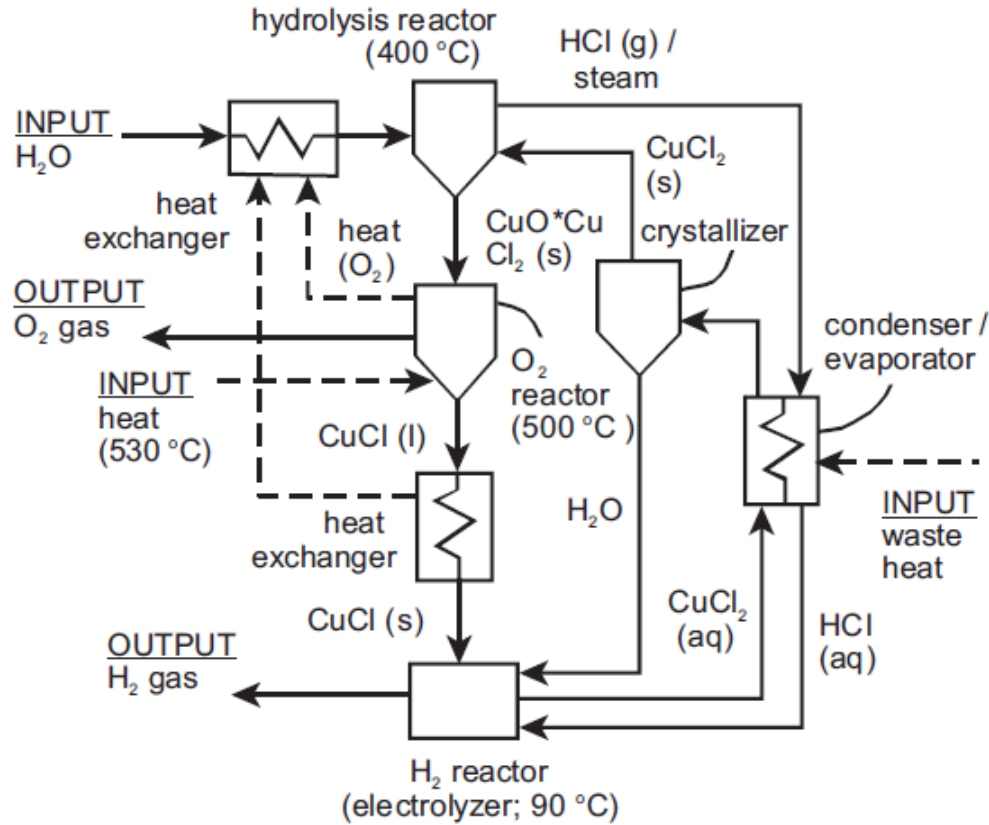


Figure 1.1: Schematic of the operation of Copper Chlorine cycle [10]

In this research, the hydrolysis reaction is the focus of interest. Since the reaction is heterogeneous, there are three main resistances present during the reaction. The gaseous reactant H_2O must reach the surface of the solid against the resistance of H_2O flow, which is defined as the external diffusion resistance. Then

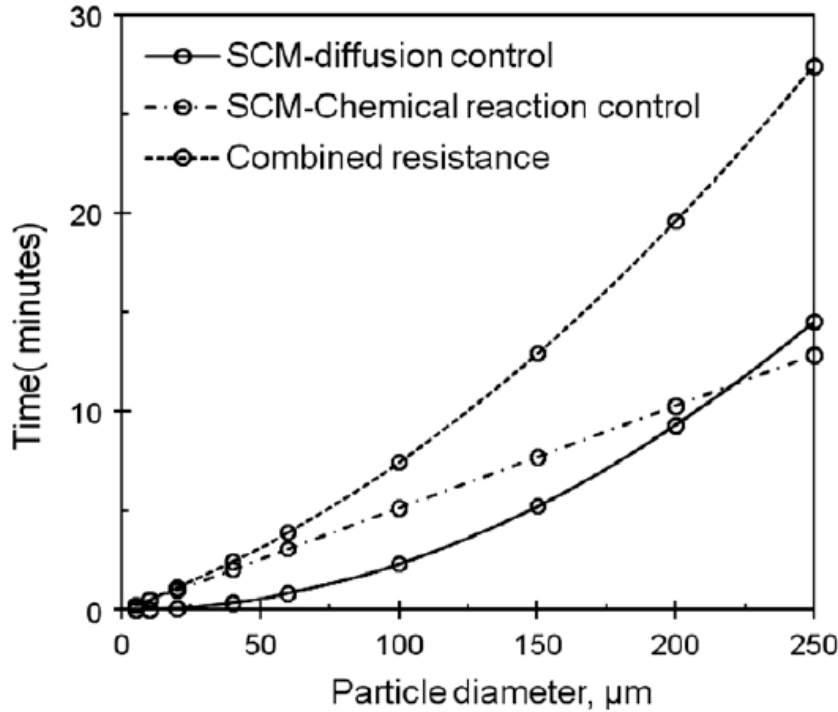


Figure 1.2: Variation of the cupric chloride conversion time with particle diameter [11]

$\text{H}_2\text{O}(\text{g})$ needs to reach the reacting surface, which is located inside the solid particle and moves inwards from the outer solid surface with time, through a reacted solid material, Cu_2OCl_2 . This product layer has a mass transfer resistance, identified as the internal diffusion resistance. Finally, once the $\text{H}_2\text{O}(\text{g})$ reaches the reaction surface, the reaction rate determines the mass flow. Therefore, the resistance from the reaction surface becomes the final resistance, defined as the surface reaction resistance [11, 12].

The external diffusion depends on various parameters, including the $\text{H}_2\text{O}(\text{g})$ flow, external diffusion constant and particle size. The internal diffusion varies with respect to the particle size, internal diffusion coefficient and concentration of $\text{H}_2\text{O}(\text{g})$ at the outer surface. The rate of reaction depends on the reaction rate coefficient and concentration of $\text{H}_2\text{O}(\text{g})$. Thus, the surface reaction resistance against mass transfer also depends on several parameters. The resultant resistance for the mass transfer is a summation of all three resistances. But the relative magnitudes of each resistance control the overall resistance. Therefore, the mass transfer resistance can be considered as the controlling resistance. Figure 1.2 demonstrates the differences between each resistance for conversion time with respect to particle diameter [11, 12].

The magnitudes of resistance change with the particle size. The external diffusion resistance could be

considered negligible with respect to the other two resistances at higher flow rates of the reactant gas, steam. For a larger particle size, the internal diffusion resistance becomes larger since there is more distance and space for the reactant gas to pass through the product layer with larger particle sizes. For smaller particle sizes, the surface reaction is larger because the reaction surface is insufficient for a faster reaction rate with small particle sizes. Therefore, in a range of particle sizes, an effective particle size exists in which the controlling resistance changes from one to the other [11,12].

The thermophysical properties, which include the reaction rate constant and internal diffusion constant, are the most important to determine the effect of internal diffusion resistance and surface reaction resistance, leading to an effective particle size. In past literature, the mentioned parameters are calculated through approaches of modeling reactions. The available experimental data is rare. The main objectives of the research are to determine the corresponding thermophysical properties and effective particle size at operational conditions of the hydrolysis reaction.

1.1 Objectives and Expected Contributions of the Research

The main objectives and contributions of the research are listed below.

Objective 1: Determine the effective particle size and its variation to understand the mass transfer controlling step.

- Observation of hydrolysis reaction and comparison of proposed concept to determine reaction kinetics. To the best of the author's knowledge, the total conversion time and respective resistance types for evaluating the effective particle size have not been performed previously.
- Use of all available readings and measurements to improve the accuracy and quality of results.

Objective 2: Propose to measure the selected thermophysical properties from the samples.

- The available experimental data for reaction kinetics is scarce for the hydrolysis reaction. The reaction rate coefficient and internal diffusion are determined from the experimental data.

Objective 3: Analyze the trends of temperature and partial pressure of compounds on the reaction kinetics.

- Atmospheric pressure and a temperature of 390 °C were maintained for the experimentation. A comparison of obtained results and previous literature values were carried out.

- Complete pressure drop calculations for the whole pipe system of the apparatus, including the effects of temperature and pressure.

1.2 Overview of the Thesis

Hydrogen production using thermochemical cycles has been a research focus for the past few decades. The potential thermochemical cycles are reviewed, and the most feasible cycles are identified. The Cu-Cl cycle is a potential and feasible thermochemical cycle. A comparison of the most viable and potential thermochemical cycles is included in Chapter 2. The reaction kinetics of the hydrolysis reaction is one of the interests as the available experimental data are limited. The necessity to gain experimental thermophysical properties was presented in the past literature. The possible undesired reactions during a hydrolysis reaction are investigated. Reaction kinetics and results of the previous studies are presented in a detailed literature review in Chapter 2.

Knowing the thermo-physical properties of the hydrolysis reaction leads to a better understanding of the reaction kinetics. The available properties derived through the experimental approach are found. The equilibrium constant, reaction rate, and order are discussed. The propagation of the reaction is analyzed with respect to the solid reactant. The concepts of different models are analyzed. The reaction rate constant and internal diffusion coefficient calculations are presented in Chapter 3.

The experimental setup has five major parts: humidifier, preheater, reactor, scrubber solution, and nitrogen tank. Tasks and configurations of each part are discussed. The operating conditions of the thermolysis reaction were considered in designing the setup. A high temperature of 390 °C and the corrosive environment caused by HCl played a major part in material selection. Measuring the respective quantities of compounds is discussed. A detailed section on the reactor bed design, pressure drop calculation of the experimental apparatus, electrical circuit, and safety assessment are included in Chapter 4.

The Data Acquisition System is presented in Chapter 5. A comprehensive section of utilized sensors and transducers and their functionality is included. The parameters for calculation are not read directly from all the readings and measurements. Therefore, the required calculation of chloride ions and pH value is included. The uncertainty of measurements is presented in Chapter 5.

The results and discussion for thermophysical properties, reaction rate, conversion, and other processes

are discussed in Chapter 6. The conclusions for the obtained results and recommendations for future research are outlined in Chapter 7.

Chapter 2

Literature Review

2.1 Hydrogen production by thermochemical cycles

Hydrogen generation is commercially available by natural gas reforming, coal gasification and electrolysis of water. The enthalpy change for the water-splitting reaction is 242 kJ/mol at standard conditions. This requires a temperature higher than 4000 °C, which requires to use of many sophisticated materials for construction. Therefore a possible solution is to use a thermo-chemical cycle for water decomposition. With the aid of Hess's law, there are more than 200 cycles, and several cycles among them have been thoroughly investigated, such as Sulphur Iodide (S-I), Magnesium Iodine (Mg-I), Cu-Cl, Cesium Chlorine (Ce-Cl), Ferrous Chlorine (Fe-Cl), Vanadium Chlorine (V-Cl), Copper Sulphate (CuSO_4) and hybrid chloride cycles. The sulphur-iodine cycle requires a temperature of 800 °C for water decomposition. The Mg-I cycle also demands higher temperature requirements than the Cu-Cl cycle. A major advantage of the Cu-Cl cycle is that a maximum temperature of 530 °C is sufficient for operation. The temperature can be supplied once combined with a geothermal, solar or waste heat source [2–5,13,14].

An High Temperature Gas Reactor (HTGR) can be used for the safe operation of electricity generation and heat utilization with hydrogen production at about 1000 °C. As mentioned earlier, the Japan Atomic Energy Research Institute developed an HTGR to demonstrate hydrogen generation of 120 m³/h. An experiment with the S-I cycle for water splitting by Shinji Kubo et al. 2004 [15] for hydrogen production of 32L/h for 20h was reported. Andress et al. 2009 [6] proposed a systematic methodology consisting of five strategies: conceptualization, reaction cluster synthesis, flow sheet design simulation and analysis, process integration and performance evaluation for evaluating alternative thermochemical cycles. Aspen Plus soft-

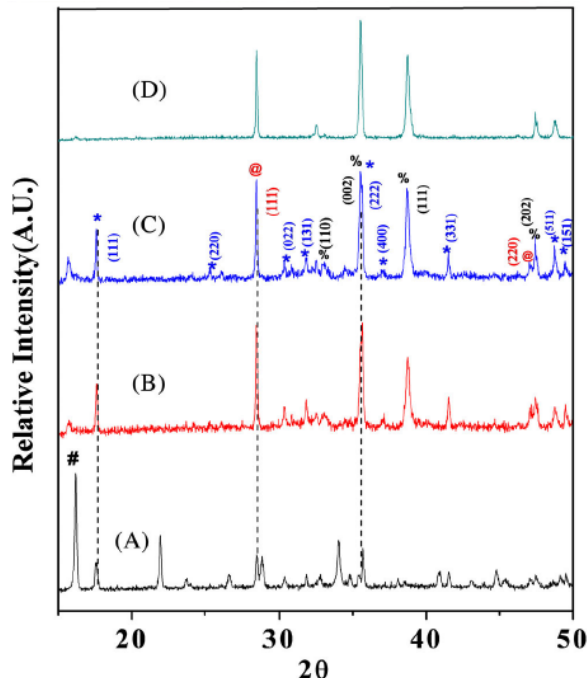


Figure 2.1: Powder XRD patterns of the hydrolysis product samples isolated after (a) 15, (b) 30, (c) 45, and (d) 60 min over [5]

ware was utilized for performance analysis. Five Fe-Cl alternative thermochemical cycles were identified as exceeding the minimum threshold efficiency of 35%. The evaluation started with a formal definition of thermodynamic feasibility, proposed automatic selection algorithm, analysis by Aspen-Plus software, pinch diagrams for heat integration and finally, a standard definition of efficiency calculations.

The Cu-Cl cycle has three main reactions of hydrolysis, thermolysis and electrolysis. Steam reacts with solid CuCl_2 to form Cu_2OCl_2 and gaseous HCl. The electrolysis reaction produces hydrogen gas and $\text{CuCl}_2(\text{aq})$ from $\text{CuCl}(\text{aq})$ and $\text{HCl}(\text{aq})$ at a temperature between 80°C and 100°C . A temperature of 450°C - 530°C satisfies the thermolysis reaction, which decomposes Cu_2OCl_2 to $\text{CuCl}(\text{l})$ and oxygen gas. The hydrolysis reaction has attracted broad research interests. The efficiency of a hybrid Cu-Cl cycle is approximately 40% [13]. Two central problems to be addressed in the hydrolysis reaction are to prevent forming undesirable products of Cl_2 from CuCl_2 and to minimize excess steam requirements. Extra steam results in higher yields of Cu_2OCl_2 , but it also increases the heat requirement for steam generation. Therefore the ratio of steam to copper plays a significant role and will be investigated. Past XRD results of experimental products are presented in Figure 2.1 [5].

Wei Wu et al. 2018 [16] designed and evaluated on an energy basis a stand-alone two-step Cu-Cl cycle

using a CuCl/HCl electrolyzer to generate electricity together with hydrogen and oxygen combined with specific heat and power units under five different conditions. The efficiency of the cycles was found to be 48%. Considering CO₂ emissions due to power generation, the reformation of methane and oxyfuel combustion technologies were also reported. The CO₂ emissions could be limited to 0.418 kg/kWh. The pinch method and heat exchanger network were utilized to calculate the required optimum heat recovery of the cycle. The expected yield of the two-step Cu-Cl cycle was found to be between 0.452-4.39 kWh/m³ of H₂ and the efficiency was determined to be 23.77-31.97%.

Al-Zareer et al. 2020 [3] proposed a conceptual design of a generation IV nuclear reactor integrated with a four-step thermochemical Cu-Cl cycle, a Brayton cycle of Helium gas, and a Rankine cycle of steam for electricity and hydrogen production. The design was compared with Aspen-Plus software. Helium acted as the heat transfer fluid. Energy and exergy analyses were determined to have an efficiency of 14.1% and 20.7%, respectively. The configuration is capable of producing 1 mole of hydrogen at a pressure of 250 bar per every 3.7 kg/s of H₂O. It was concluded that a 600 MW gas-cooled fast reactor was able to produce hydrogen at a rate of 86.5 mol/s and 60.4 MW of electricity.

Hydrogen production by solar energy was analyzed by Abanades et al. 2006 [14]. Over 280 thermochemical cycles were considered to be driven by solar energy. The selection and evaluation processes were done to find the most promising cycles for a temperature range of 900 - 2000 °C. Nearly 30 cycles were then investigated further based on a thermodynamic evaluation. The parameters of an environmentally attractive, large-scale, low-cost, and high-efficiency product for hydrogen by using concentrated solar energy with high-temperature heat were used for the evaluation. Cycles up to three steps were found to be economically more feasible and attractive for implementation. The proposed research will include a detailed thermodynamic study of the reaction system, experimental analysis of the selected cycles and development of the flow sheets in future investigations.

Rosen et al. 2010 [4] thoroughly investigated the hydrogen processes powered by thermochemical cycles. The analysis of energy and exergy was presented in terms of efficiency. A pilot case was selected to be the Cu-Cl cycle. The limiting efficiencies related to cycles were calculated and explained. One of the main advantages of using a thermo-chemical cycle for hydrogen production was the low temperature required by the other conventional methods and the capability of operating with various heat sources. Therefore, lowering the peak temperature of existing cycles and searching for low-temperature alternative cycles had to be continued. The Cu-Cl cycle needs a temperature of less than 550 °C which is considerably lower compared

with other cycles. The challenges for the Cu-Cl cycle were identified as related to the reactions with particle mixing, heat exchangers operating in extreme conditions, preventing CuCl_2 particle evaporation and comprehensive knowledge of the solubilities of $\text{CuCl}_2(\text{s})$ and Cu_2OCl_2 in the mixture of HCl and steam.

A summary of the potential of nuclear energy for producing hydrogen at an industrial level was presented by El-Emam et al. 2020 [17] for five cycles: S-I cycle, Hybrid Sulfur cycle, Cu-Cl cycle, Mg-Cl cycle, and Ca-Br cycle. The S-I cycle demonstrated a capability of large-scale hydrogen production at high efficiency with a competitive cost but a few drawbacks of uncertainties related to chemical kinetics and thermodynamics. The availability of Iodine worldwide is a limitation to be considered. The hybrid Sulfur cycle must be further improved in electrolysis for a lower cell potential of SO_2 depolarized water electrolysis, as well as prevention of SO_2 crossover during the process and also a capability to operate under low operating potentials before commercial production. In addition to recent progress in the Cu-Cl cycle, a pilot plant for the operation was proposed. For the Mg-Cl and Ca-Br cycles, significant uncertainties are associated with reaction kinetics and thermodynamics.

The capability of using waste heat from a cement plant for the Cu-Cl thermochemical cycle for hydrogen production was presented by Odukoya et al. 2014 [18]. A design of a calcium oxide / steam chemical heat pump was presented within the study. The waste heat was used to provide energy to the thermolysis reaction for the decomposition of Cu_2OCl_2 . The optimal decomposition pressure and evaporator pressure were determined to be 3.67 bar and 0.042 bar, respectively, for a range of flue gas temperatures.

2.2 Cu-Cl Thermochemical Cycle

The chemical and physical steps in the CuCl thermochemical cycle are hydrogen production (Step 1), electrochemical process (Step 2), drying step (Step 3), hydrogen chloride production (Step 4), and oxygen production (Step 5). Input water is added externally in Step 4. Then water reacts with CuCl_2 and produces $\text{HCl}(\text{g})$ and Cu_2OCl_2 at a temperature between $350 - 400^\circ\text{C}$. The gaseous product, HCl, is heated up to $430 - 475^\circ\text{C}$ and reacted with Cu as per Step 1 in the hydrogen production reaction. This yields hydrogen gas and molten CuCl as the products. The remaining product of the hydrolysis reaction, Cu_2OCl_2 is also heated and transferred to the oxygen production reaction, which is Step 5 at a temperature of 530°C , resulting in oxygen gas and molten CuCl. The Step 1 and 5 products, CuCl, are transferred to Step 2, the electrochemical step to produce $\text{Cu}(\text{s})$ and $\text{CuCl}_2(\text{aq})$ at ambient temperature. $\text{CuCl}(\text{aq})$ will be dried before transferring to Step 4. Hydrogen chloride is produced, and $\text{Cu}(\text{s})$ is transferred to the hydrogen

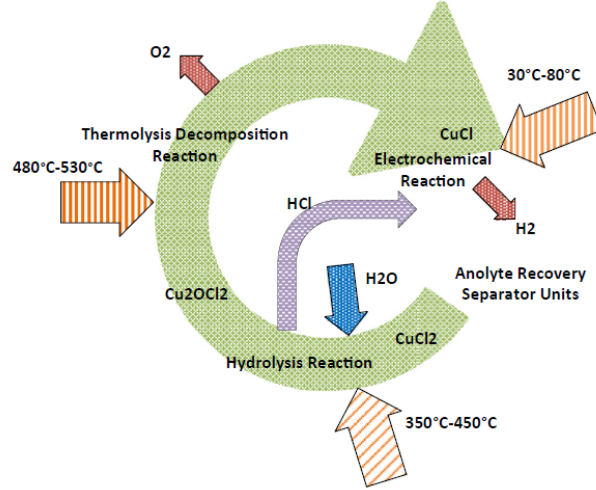
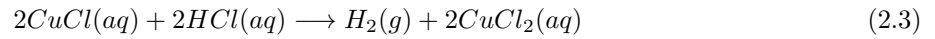
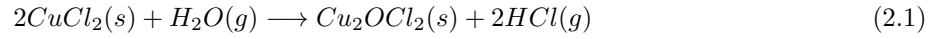


Figure 2.2: Schematic representation of the Cu-Cl cycle [19]

production, Step 1. The cycle operates in a cycle, provided with water, heat, and electricity externally, and inner products are recycled [2]. The schematic of the Cu-Cl cycle is shown in Figure 2.2. The hydrolysis, thermolysis, and electrolysis reactions are demonstrated in equations 2.1, 2.2, and 2.3, respectively.



The integration of hydrogen production via the Cu-Cl thermochemical cycle with a Generation IV nuclear reactor, a Super Critical Water Reactor (SCWR), was reviewed by Naterer et al. 2011 [20]. Individual units and their connections to the cycle were examined with industrial waste heat or solar energy as the energy input. It was found that the efficiency of hydrogen generation with SCWR increases to 42% resulting in approximately 30% net efficiency when including electricity generation and electrolysis. For the CuCl and HCl electrolyzer, new membranes developed with lower copper diffusion rates than Nafion were presented. The powder characteristics, membrane permeability, and conductivity measurements were reported. Canadian Nuclear Laboratories demonstrated a stable cell performance at voltages down to 0.477 V for 10 h of the CuCl and HCl electrolyzer .

The feasibility of process integration of hydrolysis and electrolysis reactions in the Cu-Cl cycle was examined by Aghahosseini et al. 2013 [21]. This corresponding integration is one of the most important challenges

of the cycle. The intermediate heat recovery steam generator and separation process for water vapour and HCl were used for analyzing the internally coupled processes of rectification and absorption. The minimum allowable energy input was taken as a criterion. The feed flow rate was 18 kmol/h, accompanied by 13.5 mol% and a temperature of 90 °C. It was found that the HCl concentration can be increased by 10% with 30% incremental heat input by increasing the reflux ratio by 50% for a constant product flow rate. The steam requirement is 14 times the stoichiometric value for the hydrolysis reaction with the heat recovery steam generator system.

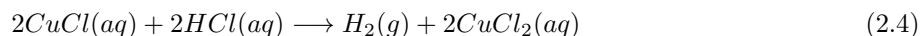
A multi-objective optimization of the Cu-Cl thermochemical cycle with an artificial neural network for hydrogen production was analyzed by Farsi 2020 et al. [19]. An artificial neural network used machine learning. Aspen Plus software was used to model the integrated process, including the kinetics of the hydrolysis reaction over a range of operating conditions. The thermodynamic assumptions were steady-state operation and reference environment conditions of 25 °C and atmospheric pressure. An energy and exergy analysis was performed with the experimental study according to the first and second laws of thermodynamics. Also a cost analysis was completed by taking the operating expenses for units in the cycle. The operation cost was decreased, and exergy efficiency was increased, at an increasing operating temperature, average temperature of recovery units, Steam to Copper (S/Cu) molar ratio and pressure swing distillation unit temperature. The results were analyzed by a Pareto front sensitivity analysis .

Razi et al. 2020 [22] presented a thermal management system for the integrated lab-scale Cu-Cl cycle through an energy and exergy analysis for six different steam and heat recovery configurations in which the S/Cu ratio varied for each configuration. To determine the performance of a configuration, the criteria of exergy destruction of the heater, net energy and exergy input, temperature after heat recovery, and overall system energy and exergy efficiencies, were studied. The highest energy and exergy efficiencies were 6.8% and 10.4%, respectively, when heat recovery is absent, and corresponding values were 10.7% and 16.3%, respectively, with a heat recovery system present. Hydrogen production rates varied between 2.30 kg/h and 3.58 kg/h.

Sayyaadi et al. 2017 [23] showed a novel conceptual design of a solar Cu-Cl cycle for a production rate of 3000 kg of hydrogen per day. Thermal management was used to improve thermal efficiency and heat recovery. A pinch analysis was used to design the corresponding heat exchangers. Several criteria were considered to optimize the design: three objective functions - energy, exergy and unit cost analysis and one multi-objective function, which includes thermodynamic, solar thermal and exergoeconomic analyses. The design shows a

thermal efficiency of 49.83 %, exergetic efficiency of 58.23 % and unit cost of 6.33 \$/kg .

The electrolysis reaction is one of the main steps within the Cu-Cl cycle. It is denoted by Equation 2.4. Aghahosseini et al. 2013 [24] presented experimental data from a lab-scale Cu-Cl process with an analysis of the effects of operating parameters such as HCl and CuCl concentrations, solution flow rate, temperature, applied current density and hydrogen production rate. The design was two-level factorial and its accuracy was examined by an ANOVA analysis. The higher HCl concentration and current increased the cell voltage, while higher flow rates and temperatures reduced the cell voltage. An analysis of HCl concentration and current density with flow rate was discussed. The cell current efficiency was evaluated to be about 93%.



Despite the advantages of the Cu-Cl thermochemical cycle, challenges are also present. Various examined areas were addressed by Ghandehariun et al. 2012 [25]. The paths where the Cu-Cl cycle has challenges were considered, such as the thermolysis decomposition reaction, heat recovery, solidification, and dissolution. The minimization of CuCl generation was discussed and evaluated regarding process integration, heat recovery, and design factors. There were promising solutions for absorbing CuCl vapour, such as cooling the gases at the thermolysis reactor exit. This was later determined to be undesirable due to clogging of oxygen flow, utilizing water vapour or CuCl₂, and integrating additional equipment into the cycle. The use of Cu₂OCl₂ for the thermolysis step was a preferable approach.

In terms of the lowest cost, thermal and power requirement, energy, and exergy efficiency, Mehrpooya et al. 2020 [26] conducted a performance analysis for thermochemical water splitting including the S-I cycle, Zn-S-I cycle, Cu-Cl cycle, Mg-Cl cycle and Fe-Cl cycle as shown in Table 2.1. Rajasekaran et al. 2021 [27] performed an analytical prediction of the thermodynamical property of heat capacity for molten salts, CuCl and AgCl, combined with the Cu-Cl thermochemical cycle.

Molten CuCl is subjected to heat recovery resulting in a temperature from 450 °C to 90 °C. With dissolved HCl it then produces H₂ in the electrolysis step. Since there is limited information on the properties of molten salts, a new model was proposed based on available thermal data. Debye's model, in which the vibration of crystals due to heat addition is included, is considered for temperatures less than Debye's temperature, 280 °C. From 280 °C to the melting point, the heat capacity was derived with the assistance of experimental results and simulation results. Beyond the melting point, the heat capacity was calculated

using the Gibbs-Helmholtz relation as supported by thermal data [27].

Table 2.1: Performance comparison of thermochemical cycles

Cycle	Energy Efficiency (%)	Exergy Efficiency (%)	Pros	Cons
S-I	46.9	62.9	High Efficiency, No electricity requirement, Low cost.	High temperature requirement, Formation of azeotropes
Zn-S-I	57.0	-	Conversion of CO ₂ to CO addition to H ₂	High energy requirement, Number of associated reactions.
Cu-Cl	44.3	78.2	Low maximum temperature, No catalysts required, Low cost.	Electricity requirement, Electrochemical cell development.
Mg-Cl	55.4	53.0	Maximum low temperature.	Mg reacts and produces a layer of products covering surface.
Fe-Cl	37.0	-	Inexpensive chemicals, Extensive knowledge of iron oxides and chlorides.	Low efficiency, Low yield of reverse Deacon reaction.

A separate predictive model for heat recovery from molten CuCl for the Cu-Cl cycle was presented by Jaber et al. 2010 [28]. A counter-current spray flow heat exchanger was utilized, and the convective heat transfer between molten CuCl droplets and the air was analyzed. Effective thermal management can increase thermal efficiency, by heat recovery internally within the cycle. The predictive model was used for unit a heat exchanger of 0.13 m diameter and heights of 0.6 m and 0.8 m.

The viability of replacing the electrolysis sub-system with a hybrid photocatalytic-based reactor was determined by Ratlamwala et al. 2018 [29] at ambient temperature and variable reactor temperature, current density and electrode distance. Results showed that the exergy efficiency was decreased from 5.25 % to 3.9 % when increasing the ambient temperature. The increase in current density decreased the energy and exergy efficiencies from 5.74 % to 4.54 % and 5.11 % to 4.04 %, respectively. As per the predicted results, the hybrid reactor can replace the electrolysis sub-system and improve the Cu-Cl cycle.

Gevez et al. 2022 [30] presented a study of a design of an integrated system with a geothermal energy source and the Cu-Cl cycle. The renewable energy system can produce hydrogen and fresh water through a multistage desalination system. The concept of utilizing heat pumps to achieve high temperatures in the thermochemical cycle is discussed. Five outputs are generated from the design: hydrogen, fresh water, hot water, heat for space heating and electricity. The mercury-cascaded heat pumps have a coefficient of performance of 1.557 for energy and 1.228 for exergy. The system generates a net electricity output of 8.277 kW at a freshwater rate of 47.9 kg/s and 7.3 kg/hr. The addition of geothermal energy increases the energy and exergy efficiencies by 42.1 % and 48.7 %, respectively.

An analytical method was proposed by Bolükdemir et al 2018 [31]. for calculating the thermophysical properties of Cu, CuO and CuCl in the Cu-Cl cycle. The Debye function is used to solve for all temperature ranges using statistical thermodynamics. The results agreed with available literature values for low and high temperatures.

The compatibility of materials for the Cu-Cl cycle was experimentally examined for metal alloys, Alloy 686, Inconel 625, Alloy 22, Incoloy 825 and 316 stainless steel, and Hastelloy N by Nijhawan et al. 2022 [32]. A constant temperature of 450 °C was generated by the furnace in which the experimentation was performed. CuCl vapour was generated by heating 60 g of solid CuCl. The furnace is heated up, and the available oxygen level is used to calculate the oxidization of materials. According to the results, nickel-based alloys have less oxidation than 316 stainless steel in a CuCl-containing atmosphere.

Wu et al. 2016 [33] evaluated the economics of the three-step CuCl cycle. The proposed layout consists of an O₂ production unit, H₂ production unit, and a CuCl electrolysis unit. To increase energy and cost-effectiveness, a heat recovery system is added to the system, increasing the energy efficiency by 33.87 % to 47.31 %, respectively. The economic calculations were the internal rate of return and net present value. The results show that the labour cost is the largest among the operational costs while the operating cost is the highest overall.

Asal et al. 2021 [34] investigated the compatibility of thorium molten salts for the Cu-Cl hydrogen production potential for the three-step Cu-Cl cycle using a neutronic analysis. There were six cases with different ratios between ThF₂ and the coolant Li₂BeF₄ deviating ThF₂ from 98% to 88% by 2%. The results show that the TF₄ fueled laser inertial fusion driven reactor has the potential to integrate a three-step Cu-Cl cycle.

2.3 Reaction Kinetics

Daggupati et al. 2010 [11] investigated the CuCl_2 conversion in the heterogeneous hydrolysis reaction to determine the reaction rate constants and total time for complete solid conversion by using a shrinking core model for a fluidized bed of uniform particle sizes. It was considered solid particles (spherical) with a size of 200 microns. The chemical equilibrium and heat input requirements were used to examine the hydrolysis reaction with varying effects from an inert gas, pressure, excess steam, temperature, and HCl in the steam. The complete conversion of reactant CuCl_2 could be obtained at a temperature of 375°C at operating conditions for pressure and inert gas supply. HCl production increases with incremental excess steam. The maximum HCl amount depends on the inert gas's temperature and composition. The chemical reaction control step and diffusion through the product layer control were investigated.

2.3.1 Parallel Reactions

Daggupati et al. 2010 [7] investigated the solid reactant hydrolysis and decomposition in the Cu-Cl cycle taking external parameters such as S/Cu ratio, temperature, and pressure into consideration in equilibrium conditions under the shrinking core model. Decomposition occurs at temperatures higher than 400°C . The temperature for hydrolysis begins between 350°C and 400°C . The decomposition and hydrolysis reactions are represented in equations 3.3 and 3.2, respectively. The equilibrium favours the higher temperatures. Nevertheless, higher temperatures also increase the decomposition of solid reactants and Cl_2 formation.



The thermolysis reaction of the Cu-Cl cycle produces oxygen at temperatures higher than 450°C . The thermal management inside the reactor is crucial as the product of the hydrolysis reaction tends to react again and produce unwanted products within the hydrolysis reactor. Wajda et al. 2019 [35] investigated a novel thermolysis reactor design - a pilot design scaled up according to the industrial application. The analysis was performed with the available experimental data and simulation data — for the reduction of temperature of CuCl vapour forming during the heating process. The setup with a dual heater configuration ensured that a production rate of 100 kg H_2 per day in a cycle has the capacity to proceed with 10.6 kg.

Thomas et al. 2011 [9] carried out an experiment for the reaction kinetics of thermolysis on an equimolar mixture of CuO and CuCl_2 , and Cu_2OCl_2 produced after hydrolysis for a temperature range of 470°C - 575°C . The O_2 yield was reported to be significantly decreased for temperatures higher than 500°C due to

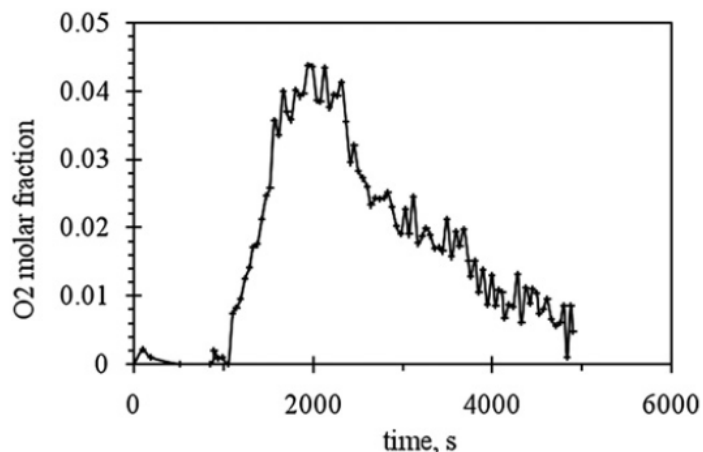


Figure 2.3: Oxygen generation by decomposition of Cu_2OCl_2 at 490°C and 1.003 bar [9]

the occurrence of the intermediate step of CuO chlorination. At higher temperatures, molten CuCl starts to chlorinate, and diffusion of Cl_2 affects the overall thermolysis reaction [8]. The oxygen generation by the decomposition of Cu_2OCl_2 is shown in Figure 2.3.

The energy performance of the electrolysis reaction of the Cu-Cl cycle of three, four, and five-step configurations and the Brayton cycle for hydrogen and oxygen production was evaluated by Wu et al. 2017 [36] using Aspen Plus software. The criteria for analysis were based on the effects of temperature and pressure on the yield of Cu_2OCl_2 and CuCl in the hydrolysis and thermolysis reactions, effects of steam ratio on energy efficiency and Cl_2 production, and internal heat recovery ratio. The configuration increased the internal heat recovery ratio for the three-step Cu-Cl cycle and 72% for the five-step Cu-Cl cycle.

An X-ray diffraction analysis of molten CuCl and O_2 was presented by Marin et al. 2011 [9] for the decomposition of Cu_2OCl_2 . This study identified the operating conditions that demote the reverse reaction of thermolysis. The equilibrium for the highest conversion of Cu_2OCl_2 was found to be at temperatures higher than 500°C and pressures below 2 bar. The optimal temperature was determined at conditions where the temperature is between 500°C and 525°C and pressures between 1 bar and 2 bar.

2.3.2 Pressure Drop of Packed Bed

Pope et al. 2011 [37] studied the fluid flow characteristics through a packed bed reactor used for hydrolysis. The pressure drop of the packed bed was critical for improving the system efficiency for different materials with various sphericities having particle diameters of $450\mu\text{m}$, 4mm, and 1cm. The flow conditions were investigated for regions of Reynolds number between 20 and 150. The Ergun equation showed agreement

for the above region. Flows with a Reynolds number below 20 were affected by frictional forces since the particles were small.

2.3.3 Energy and Exergy Analysis

Orhan et al. 2005 [38] analyzed energy and exergy models considering 1kJ/mol of hydrogen production under reaction environments of room conditions, steady state, and adiabatic. Once the reaction temperature increases from 100 to 1000°C, then reaction heat increases from 101MJ/kmol H₂ to 108MJ/kmol H₂, while at 400°C, the reaction heat is determined to be 105,266 kJ/kmol H₂. The exergy destruction was calculated to be 68MJ/kmol H₂ for the fluidized bed when the reaction temperature is 400°C, and the reference environment temperature is 25°C. The exergy efficiency is estimated to be 76% at a reaction temperature of 400°C. This efficiency decreases with increasing reference environment temperature and reaction temperature .

A detailed second law analysis of the hydrolysis reaction was presented by Farsi et al. 2020 [39] for gas-solid reacting flow considering thermal and chemical irreversibilities of the spray reaction process. The most influential parameters for the hydrolysis reaction were the S/Cu ratio, operating temperature, and reaction kinetics in evaluating the exergy efficiency. Although higher temperatures favoured the higher conversion of reactants, the preheating of solid reactant and water vapour led to significant exergy destruction from 60.3 MW to 106.5 MW at an operating temperature of 380 °C. The maximum exergy efficiency was reported for a S/Cu ratio of 30 at 380 °C while for a S/Cu ratio of 5 at 450 °C. The optimum operating temperature was 388 °C, and the S/Cu ratio was 19 for the optimum operation of the hydrolysis reactor, according to the results.

2.3.4 Limiting Thermodynamic Efficiencies of Thermochemical Cycles

The Carnot efficiency equivalence was defined by Ewan et al. 2006 [40] for 21 reported cycles to determine the limiting efficiency for further cycle implementation and development. The maximum allowable internal heat transfer is investigated to minimize the external heat input to the cycle. Out of 21 cycles, the Ispra Mark 1C process obtained the highest efficiency of 69%.

2.4 Experiments and Results

A detailed study of the hydrolysis reaction was conducted by Singh et al. 2020 [5] to understand the behaviour of corresponding compounds such as Cu₂OCl₂ and CuCl₂. Reaction parameters of temperature,

S/Cu ratio, flow rate, reaction duration, and particle size were considered. The experiment was a fixed bed reactor, and the carrier gas was nitrogen and argon. Commercial $\text{CuCl}_2 \cdot 2\text{H}_2\text{O}$ with an analytical reagent of 98% was heated in an oven to obtain anhydrous CuCl_2 for two to three hours. The colour of the compound was found by changing from sky blue to brown. The reaction extent of hydrolysis was measured by acid-base titration of HCl and stoichiometry of the reaction. The results were confirmed by Thermo Gravimetry - Mass Spectrometry (TG-MS), temperature-programmed desorption, and linear combination fitting of extended X-ray absorption fine structures. It was qualitatively verified by scanning electron microscopy, X-ray diffraction and Extended X-ray Absorption Fine Structure (EXAFS) .

XRD patterns of dihydrate $\text{CuCl}_2 \cdot \text{H}_2\text{O}$, anhydrous CuCl_2 , Cu_2OCl_2 and $\text{Cu}(\text{OH})_3\text{Cl}$ were found to crystallite in the eriochalcite phase with an orthorhombic lattice, monoclinic lattice, melanothallite phase and atacamite phase, respectively. Reaction duration played a significant role in the product evaluation of hydrolysis reactions. The main output was Cu_2OCl_2 with time increasing to a point where it changed to CuO or CuCl. Prolonged hydrolysis might cause the decomposition of Cu_2OCl_2 to form CuO. The possibility to generate CuCl was examined as CuCl_2 hydrolyzes to CuO via $\text{Cu}(\text{OH})_2$. The particle size differed by ball milling for different time intervals. For a smaller particle size, there is a higher hydrolysis yield. But for a particular particle, the yield started to decrease as mass resistance increased. SEM images were used to identify the morphology of solid reactants and products with micron-sized particles. The product Cu_2OCl_2 was kept isolated and further analyzed by techniques such as SEM, XRD, O_2 -evaluation, TG-MS, and EXAFS [5].

The steam to copper ratio can improve the hydrolysis yields and conversion rate. Values of 44, 22, 17 and 11 were taken for the S/Cu ratio. This enhances the oxidation of Cu_2OCl_2 to CuO, which is undesirable. The phases of unreacted CuCl_2 , Cu_2OCl_2 and CuCl were observed by XRD. The mass transfer was needed for a higher gas hourly superficial velocity and smaller particle size [5]. The O_2 evaluation methods were used. It was observed for H_2O and O_2 leaving on two separate occasions for each compound. H_2O was first dried out from dihydrate CuCl_2 and then lattice water of $\text{Cu}(\text{OH})_3\text{Cl}$ left at corresponding temperatures of 250 °C and 300 - 400 °C, respectively. Oxygen was found due to the decomposition of Cu_2OCl_2 to CuCl at 462 °C and the thermal decomposition of CuO to Cu_2O at 930 °C. TG-DTA plots, and TG-MS profiles, were used for the analysis. The activation energy for un-ball milled particles and ball-milled particles for 6 hours were determined to be 106 kJ/mol and 93 kJ/mol [5].

Ferrandon et al. 2010 [13] investigated the effect of reduced pressure and S/Cu ratio for operation through a fixed bed experimental setup constructed from borosilicate glass and chemicals. An XRD analysis was

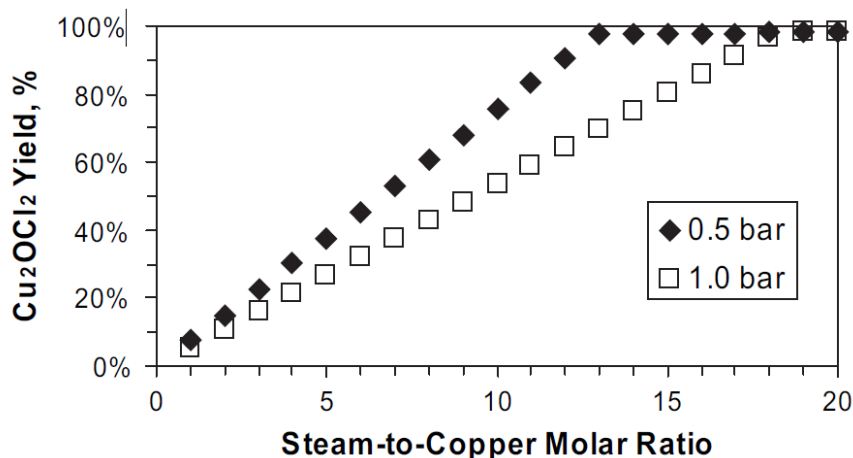


Figure 2.4: Predicted yield of Cu_2OCl_2 as a function of the $\text{H}_2\text{O} / \text{Cu}$ molar ratio at pressures of 0.5 and 1 bar [13]

utilized for measurements. The CuCl_2 solution was injected into the reactor via a continuous spray reactor by a pneumatic nebulizer. As a modification, an ultrasonic nozzle was then utilized for CuCl_2 spraying. Several thermocouples measured the temperature. An NaOH solution was used to trap exiting HCl from the fixed bed. The gas carrier was argon with 99.999% purity, and the argon flow rate was 1.60 L/min. The water was fed at a rate of 0.5 mL of liquid per hour, which resulted in 25 mL/min, enabling an adjustment of the S/Cu ratio. The aspirator and pump regulator were controlled to obtain the required reduced pressure. After the hydrolysis, the reactor temperature was decreased to 150 °C and allowed to cool further overnight with a dry air flow. The dry solid products or Cu_2OCl_2 were maintained at a temperature of 85 °C and measured by using XRD analysis and a wet chemistry method (Analytical Chemistry Laboratory). The highest conversion of CuCl_2 to Cu_2OCl_2 was obtained at a S/Cu ratio near 20. The predicted S/Cu ratio is plotted in Figure 2.4. The undesirable reaction which could occur during hydrolysis is the decomposition of CuCl_2 to CuCl and Cl_2 . The reduced pressure results in a lower formation of CuCl and maximizes the product output Cu_2OCl_2 when the S/Cu ratio is between 15 and 20.

Hydrolyzing CuCl_2 to Cu_2OCl_2 and HCl using a spray reactor was conducted by Ferrandon et al. 2010 [1]. The hydrolysis reaction's solid products were analyzed using XRD and SEM. The former approach was utilized for measuring the phase composition, while the latter was for analyzing particle sizes. A fixed-bed reactor was chosen for the experiment. The pneumatic quartz nebulizer and the ultrasonic nozzle were used with a carrier gas of argon of 99.999% purity. The product gases were subjected to bubblers containing NaOH to trap HCl . Type K thermocouples were used for measuring temperature. The amount of excess H_2O and product HCl was also measured. Chlorine was measured by an Ocean optics Ultraviolet-visible

spectrometer, while HCl trapped in the bubblers was analyzed by a pH meter. The experimental results showed that a counter-current flow design led to a higher Cu_2OCl_2 yield than a co-current flow design. A high yield of Cu_2OCl_2 was reported to be 95% conversion with a S/Cu ratio of 24 for the ultrasonic nozzle and co-current flow. An important conclusion was that Cl_2 was observed only when the reactor temperature was higher than 400°C .

The melanothallite Cu_2OCl_2 was analyzed for its magnetic properties by Kawashima et al. 2007 [41] using the μSR technique. CuO (99.999%) and CuCl_2 (99.995%) were heated at 360°C in a CO_2 atmosphere for a duration of 24h to form polycrystalline Cu_2OCl_2 . The single-phase nature of the samples was verified by powder X-ray diffraction analysis. The sample of Cu_2OCl_2 was covered with an aluminum sheet to avoid interactions with moisture and air. Spin-polarized muons and helium gas flow were used to obtain the μSR measurements. Zero-field μST spectra were taken for different temperatures between 4.1 K and 300 K. The results showed that exponential damping, and anti-ferromagnetic was displayed below 70 K.

Three separate conceptual configurations were proposed by Orhan et al. 2011 [42] for three-step, four-step and five-step Cu-Cl thermo-chemical cycles and the efficiencies of each cycle were evaluated to be 41%, 43% and 44%, respectively. The fractional parameter yield was defined as the ratio of the actual yield to the stoichiometric yield. The percentage yield was defined as the percentage value of the fractional yield, where yield was the amount of product in a chemical reaction. The overall energy efficiency was calculated as the ratio of the lower heating value of hydrogen to a total heat input which is the energy used by the process to generate a unit amount of hydrogen, and the heat loss. The second law efficiency was determined by the ratio of the total specific exergy entering to that going out. The reaction heat of HCl was found to be varying in a linearly decreasing manner with reaction temperature for any fractional yield. Future work was suggested in the area of detailed analysis and comparisons of new configurations for the Cu-Cl cycle.

Integrating the Cu-Cl cycle with waste heat of nuclear power plants is also an ongoing research topic. A system for the co-generation of electric power and compressed hydrogen from nuclear energy was proposed by Al-Zareer et al. 2017 [43]. The four-step Cu-Cl cycle was used for splitting water. The electric power generation was accomplished by the Rankine cycle. The thermal energy from the nuclear power plant based on the supercritical water-cooled reactor was supplied only to the hydrolysis and thermolysis reactor. The energy and exergy analyses were conducted based on the evaluation results of the Aspen-Plus simulation. The conservation of mass, energy and exergy in steady-state conditions was considered for evaluating system performance. The corresponding energy and exergy efficiencies were determined to be 31.6% and 56.2%,

respectively. The cogeneration power plant was evaluated to produce 553 MW of electric power and highly compressed hydrogen production at 2.0 kg/s at 700 bar .

Zamfirescu et al. 2010 [44] determined the thermophysical properties at ambient pressure of the four compounds, which are Cu_2OCl_2 , CuO , CuCl_2 , and CuCl , respectively in the Cu-Cl hydrogen production cycle. It considered thermal energy as the primary input with electricity generation for the electrolysis reaction of a system containing the reactors, heat exchangers, electrochemical cell and spray dryer. The correlation with a spray temperature from 675 - 1000 K was determined by the properties of density, specific heat, enthalpy, entropy, formation enthalpy, Gibbs free energy, and free energy.

Table 2.2: Standard thermophysical properties of CuCl Cycle-related compounds

Thermophysical property	CuO	CuCl₂	CuCl	Cu₂OCl₂
Density(kg/m ³)	6450	3420	4136	4080
Heat capacity(J/mol K)	42.27	70.71	53.34	116.77
Enthalpy of formation(kJ/mol)	-150.06	-205.85	-138.07	-384.65
Entropy of formation(J/mol K)	42.59	108.07	87.30	154.35
Gibbs free energy of formation (kJ/mol)	-128.292	-173.826	-120.876	-369.7

Reaction kinetics and transient conversion efficiencies were analyzed from the experimental results by Pope et al. 2012 [45] for packed bed reactors. A horizontal and a vertical reactor were used for the experiment in which the steam conversion was thoroughly investigated. The difference between the two separate reactors was the piping between the reactor and humidifier, resulting in higher than ambient temperatures. Nitrogen was taken as the carrier gas. Three methods were used to calculate the reaction rate based on the volume of solid reactants and the volume of gaseous reactants with two different water vapour densities of 0.59 kg/m³. The results of the vertical reactor for the operating temperature at 390 °C are used for validating the experiment. A detailed study of the experimental errors and uncertainties followed the research, including bias and precision errors. Cl_2 and HCl production is anticipated in the hydrolysis reaction. NaOH scrubber solution neutralizes HCl acidic gas released into the surroundings. The HCl reacts with NaOH as per Equation 4.12, and Cl_2 reacts as per Equation 5.2 for assisting in determining the formation of Cl_2 and HCl and their respective amounts.

Results of an integrated hydrolysis reactor at the Clean Energy Research Laboratory, University of Ontario Institute of Technology, were presented by Gabriel et al. 2019 [46]. In the study, 13.6 kW of thermal energy was provided from a Split Tube Furnace to obtain the center-line temperature of 400 °C for 500 g -

550 g of CuCl_2 and 900 g - 1000 g of H_2O . The gaseous product, HCl , was measured with pH values of -0.21 and -0.48. The nitrogen gas was the carrier gas. The solid product, Cu_2OCl_2 , was measured with XRD analysis. Both pH and XRD results suggested that a yield could be obtained between 7% - 10%.

The effectiveness of a carrier gas N_2 for reducing steam requirements was studied by Pope et al. 2013 [47]. The N_2 gas is hydrated and subjected to flow through a vertical reactor to perform the endothermic hydrolysis reaction at a temperature range of 365°C - 400°C . The theories of the Gibbs reaction energy were considered to calculate the maximum steam conversion the steam. The results were compared with the reaction quotient. The reaction temperatures were 400°C , 390°C , and 365°C . The duration of the experiments was from 0.5 h - 2.0 h. The steam requirement could be reduced to between 3.0 and 0.5 on a molar basis. It was accompanied by a minimum chlorine gas production. The elimination of the energy consuming process of separating HCl and H_2O was proposed after the hydrolysis reactor to improve conversion efficiencies.

Ishaq et al. 2019 [48] evaluated the energy and exergy efficiency by comparing three different configurations depending on the steps of Cu-Cl cycles using the Aspen Plus Software. The parameters of heat and work requirements, exergy destruction rate, and efficiencies of energy and exergy, were reported. Exergy destruction was highest for the hydrogen production reaction. In the four-step Cu-Cl cycle, exergy destruction resulted in 194.5 kW and 163.1 kW for the thermolysis reaction and hydrolysis reactions separately. The energy and exergy efficiencies were found to be 41.9% and 75.7%, respectively. For the five step Cu-Cl cycle, energy and exergy efficiencies were 38.8% and 70.2%, respectively. The three step Cu-Cl cycle had an energy efficiency of 39.6% and 68.1%, respectively.

The Cu-Cl cycle has been an extensively studied process. The reaction kinetics is a current ongoing interest in the cycle. The corresponding thermochemical properties and their behavior must be identified to analyze the operation inside the cycle. These properties are determined by modeling the reactions. Reliable experimental results are scarce on the properties. In this research, one of the objectives is to determine the related thermochemical properties and respective reaction kinetics.

Chapter 3

Hydrolysis Formulation

3.1 Hydrolysis Reaction

Hydrogen is a promising sustainable energy carrier to support growing global energy needs in the future. In this chapter, the hydrolysis reaction of the Cu-Cl cycle will be analyzed. Other well-known thermochemical cycles for hydrogen production are S-I, Mg-I, Cu-Cl, Ce-Cl, Fe-Cl, V-Cl, CuSO₄ and hybrid chloride cycles. The Cu-Cl cycle's ability to work at relatively low temperatures (530 °C) is an advantage as one of the most promising thermochemical cycles. Hydrogen has 120 MJ/mol approximately. In the hydrolysis reaction, one of the steps inside a Cu-Cl thermochemical cycle, the endothermic enthalpy balance is 105.2 kJ/mol of H₂O at ambient conditions. The reaction rate coefficient and activation energy are 2.84 h⁻¹ and 93 kJ/mol, respectively [5]. The analysis of reaction kinetics can be approached in two ways, by the progressive core model and the shrinking core model. Both models are discussed in this chapter. The latter is the more appropriate model to analyze the hydrolysis reaction.

3.2 Progressive Core Model

In this approach, the particle reacts at different locations throughout the particle during the whole conversion of the solid. Therefore the solid reactant is converted progressively and continuously throughout the particle, as shown in Figure 3.1.

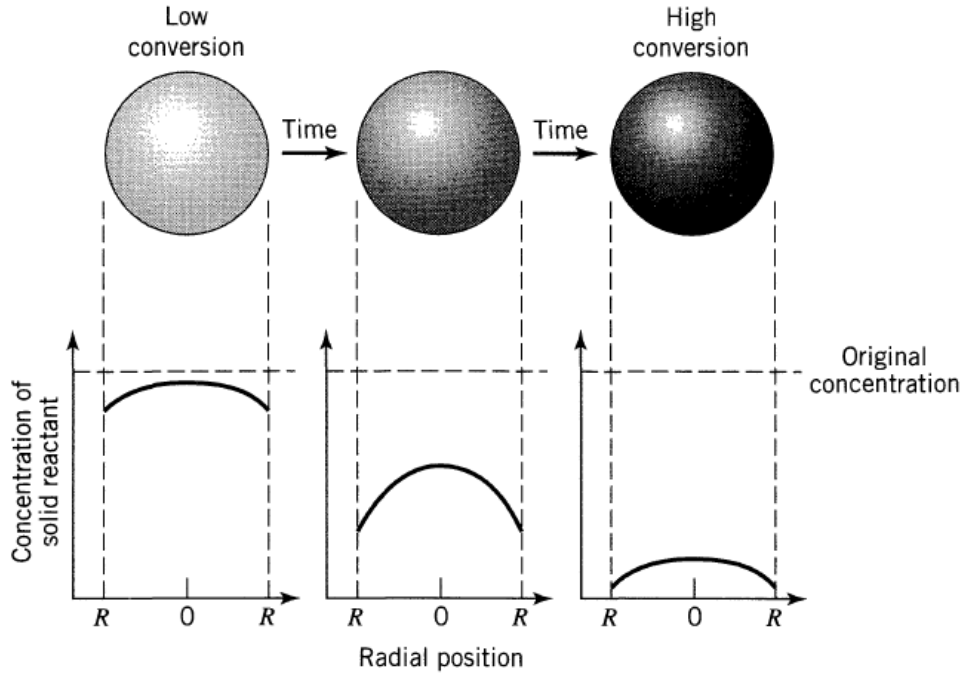


Figure 3.1: Solid reactant particle modelled in a progressive core model [12]

3.3 Shrinking Core Model

Once the reaction starts to occur, initially, the reaction happens at the outermost surface of the particle. The reaction surface gradually moves inwards to the center of the particle. The reacted material might stay a solid around the particle, which is called "ash" or the product layer. The reacted material might be all gases without leaving any trace behind the particle. In both cases, the reaction surface shrinks the unreacted core inwards. The concept is illustrated in Figure 3.2.

3.4 External Diffusion Resistance

The external diffusion, also known as gas film diffusion, varies with respect to various parameters such as fluid properties, the relative velocity between the particle and the flow, and particle size. Considering the smaller particles with a higher gas velocity increases the external mass transfer coefficient. It can be understood by Froessling's equation 3.1 for mass transfer in a fluid to free-falling solids where k_g , d_p , y , D_e , Sc , Re , μ , ρ , D_{eff} , and u are external diffusion coefficient, particle diameter, mole fraction, internal diffusion coefficient, Schmidt number, Reynolds number, dynamic viscosity, density, effective internal diffusion coefficient, and velocity of external gas, respectively.

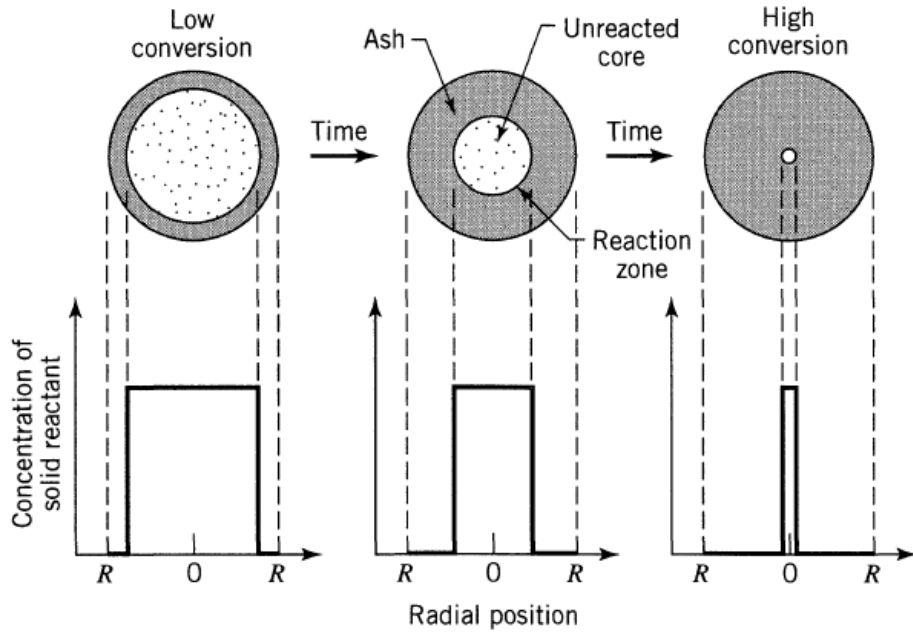


Figure 3.2: Solid reactant particle modelled in a shrinking core model [12]

$$\frac{k_g d_p y}{D_e} = 2 + 0.6(Sc)^{\frac{1}{3}}(Re)^{\frac{1}{2}} = 2 + 0.6 \left(\frac{\mu}{\rho D_{eff}} \right)^{\frac{1}{3}} \left(\frac{d_p u \rho}{\mu} \right)^{\frac{1}{2}} \quad (3.1)$$

The mass transfer coefficient indicates the ability for mass diffusion to occur externally. The mass transfer coefficient is inversely proportional to the external diffusion resistance. In this research, by enabling higher velocities, the external diffusion was held under a minimum value so that it could be deemed negligible compared to other resistances.

3.5 Internal Diffusion Resistance

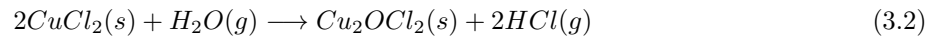
The resistance to internal diffusion takes part inside the reacted product material against the mass transfer of gaseous compounds. The mass fluxes pass through the reacted material, Cu_2OCl_2 . It is found that the rate of shrinking of the unreacted core is 1,000 times slower than the flow rate of the gas. Considering the conservation of mass, the time for complete conversion for internal diffusion can be denoted by Equation 3.24. The internal diffusion resistance is dependent on the internal diffusion coefficient, particle size, and the concentration of reactant gas at the outside surface of the particle.

3.6 Surface Reaction Resistance

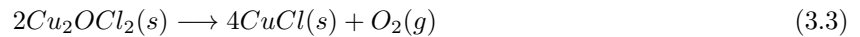
The reaction rate also plays a major part in mass transfer in heterogeneous reactions. The reaction follows stoichiometry. The reaction rate coefficient, particle size, and concentration of gaseous compound at the outside surface of the particle affect the rate of reaction. Therefore, the same properties affect the resistance at the reaction surface. The time for complete conversion will be presented in Equation 3.23.

3.7 Reaction Kinetics of Hydrolysis Reaction

The Cu-Cl hydrogen production cycle has two primary variations - a four-step Cu-Cl cycle and a five-step Cu-Cl Cycle. The hydrolysis reaction is one of the main reactions of both cycles. During this reaction, solid CuCl_2 reacts with water vapour and results in Cu_2OCl_2 and HCl , as denoted by Equation 3.2. The optimum temperature for a higher conversion of CuCl_2 is between 375 - 400°C.



Apart from the hydrolysis reaction, there are other possible reactions that could happen. The occurrence of these side reactions is undesirable for the hydrolysis process. Thermolysis and decomposition of CuCl_2 are such reactions. They are denoted by equations 3.3 and 3.4, respectively.



The thermolysis of CuCl_2 happens when the temperature is above 530°C. During experiments, the reactor temperature does not exceed 400°C. The occurrence of a decomposition reaction is monitored by checking the availability of Cl_2 emission.

The reaction kinetics for hydrolysis reaction as Equation 3.2 are modelled by using both a reversible equilibrium reaction and irreversible first-order reaction. Reaction rates for both models can be demonstrated as equations 3.5 and 3.6, respectively. The parameters \dot{r} , k , p , and K represent the reaction rate, reaction rate coefficient, pressure, and equilibrium constant of the reversible reaction, respectively. The subscripts 1 and 2 denotes being with respect to the reversible reaction and first-order reaction, respectively.

$$\dot{r}_{\text{CuCl}_2,1} = k_1 \left(p_{\text{H}_2\text{O}} - \frac{p_{\text{HCl}}^2}{K_1} \right) \quad (3.5)$$

$$\dot{r}_{CuCl_2,2} = k_2 p_{H_2O} \quad (3.6)$$

Considering the equilibrium reaction denoted by Equation 3.5, the equilibrium constant can be written as where f represents the fugacity,

$$K_1 = \frac{f_{Cu_2O} f_{Cl_2} f_{HCl}^2}{f_{CuCl_2} f_{H_2O}} \quad (3.7)$$

The pressure variation for solids is negligible with fugacity. Therefore, the fugacity effects of solids are assumed to be unity. Since steam and HCl gases are assumed to be ideal gases at the operating pressure of the reactor, which is a low pressure, the pressure of gases is equal to their fugacities for them. Hence, the equilibrium constant becomes Equation 3.8.

$$K_1 = \frac{p_{HCl}^2}{p_{H_2O}} \quad (3.8)$$

N₂ gas is used as a carrier gas to facilitate an inert gas atmosphere around the reaction surface and pressure variations of steam. When nitrogen gas passes through the humidifier, water vapour will be added to the flow. The amount of vapour in the N₂ gas is measured by a humidity sensor and controlled by a temperature controller, which is a water bath, in this experiment. Because saturation pressure is a function of saturation temperature, the saturation pressure and vapour density can be denoted as equations 3.9 and 3.10, respectively where T_H and RH represent the temperature at the humidifier and the relative humidity, respectively.

$$p_{sat,H_2O} = \frac{\exp\left(77.345 + 0.0057 \times T_H - \frac{7235}{T_H}\right)}{T_H^{8.2}} \quad (3.9)$$

$$\rho_{H_2O} = 0.0022 \times \frac{p_{sat,H_2O}}{T_H} \times \frac{RH}{100} \quad (3.10)$$

The initial pressure, temperature, and volumetric flow rate of the carrier gas, N₂, are measured to calculate the molar flow rate from Equation 3.11 assuming N₂ to be ideal where \dot{n} , \dot{V} , and M represent the molar rate, volumetric flow rate, and molar weight, respectively.

$$\dot{n}_{N_2} = \frac{\rho_{N_2} \dot{V}_{N_2}}{M_{N_2}} \quad (3.11)$$

The density of the carrier gas will be calculated from Equation 3.12.

$$\rho_{N_2} = \frac{pM_{N_2}}{RT} \quad (3.12)$$

The molar flow rate of steam is determined by Equation 3.13 in which R is the universal gas constant.

$$\dot{n}_{H_2O} = \frac{\rho_{H_2O} \dot{V}_{N_2}}{M_{H_2O}} \quad (3.13)$$

With the assistance of the extent of reaction and total pressure, the partial pressures of H₂O and HCl can be demonstrated as equations 3.14 and 3.15, respectively. N_i and X_{CuCl_2} denote the initial number of moles present and the reaction extent.

$$p_{H_2O} = \frac{N_i - 2X_{CuCl_2}}{N_i + 2X_{CuCl_2}} p \quad (3.14)$$

$$p_{HCl} = \frac{4X_{CuCl_2}}{N_i + 2X_{CuCl_2}} p \quad (3.15)$$

Thus, the equilibrium conversion of the solid reactant CuCl₂ is given as follows,

$$X_{e,CuCl_2} = \frac{1}{2} \left(\frac{K_1}{4p + K_1} \right)^{0.5} N_i \quad (3.16)$$

One of the critical parameters controlling the hydrolysis reaction is the steam to copper ratio defined by Equation 3.17 [49].

$$\xi = \frac{n_{H_2O}}{n_{HCl}} \quad (3.17)$$

Assuming solid reactant CuCl₂ particles are spherical and undergo a shrinking core model while reacting, the relationship among reaction time, corresponding conversion and completion time can be determined for CuCl₂ by considering the diffusion of steam through the particle. The CuCl₂ reaction occurs at the reaction surface between a product layer and unreacted solid core as shown by equations 3.18 and 3.19, respectively. Here t and τ refer to the instantaneous time and total time for the complete conversion, respectively.

$$\frac{t}{\tau} = 1 - 3(1 - X_{CuCl_2})^{\frac{2}{3}} + 2(1 - X_{CuCl_2}) = y_d \quad (3.18)$$

$$\frac{t}{\tau} = 1 - (1 - X_{CuCl_2})^{\frac{2}{3}} = y_r \quad (3.19)$$

An experiment will be done for varying time intervals for a specific particle size. Measuring the amount of HCl produced can determine the reacted amount of CuCl₂ as per the hydrolysis reaction in Equation 3.20.

$$\Delta n_{CuCl_2} = \Delta n_{HCl} \quad (3.20)$$

The initial CuCl₂ amount will be known. A plot of n_{CuCl_2} vs reaction time shows the complete conversion

time. Then a graph of the parameter t/τ vs X_{CuCl_2} will be plotted. If the number of time intervals is m , then the R squared value for both graphs is drawn as per equations 3.21 and 3.22,

$$R_d^2 = 1 - \frac{\sum_1^m (y_{d,i} - y_i)^2}{\sum_1^m (y_i - \bar{y})^2} \quad (3.21)$$

$$R_r^2 = 1 - \frac{\sum_1^m (y_{r,i} - y_i)^2}{\sum_1^m (y_i - \bar{y})^2} \quad (3.22)$$

Considering the R-squared value, the resistance which obtains the highest value will be determined as the controlling step. The complete conversion time for surface reaction controlling and internal diffusion controlling scenarios of the solid spherical reactant particle $CuCl_2$ are shown in equations 3.24 and 3.23, respectively. The parameters R and C represent the particle's radius and the gas concentration, respectively.

$$\tau_r = \frac{\rho_{CuCl_2} R}{2kC_{H_2O,g}} \quad (3.23)$$

$$\tau_d = \frac{\rho_{CuCl_2} R^2}{12D_{eff} C_{H_2O,g}} \quad (3.24)$$

According to the results, the k and D_e values will be calculated from equations 3.24 and 3.23, respectively.

The reaction rate of the hydrolysis reaction is calculated based on solid reactant $CuCl_2$ in Equation 3.25 where s denotes the solid reactant material.

$$\dot{r}_{CuCl_2} = \frac{1}{V_{CuCl_2}} \times \frac{dn_s}{dt} \quad (3.25)$$

The volume of $CuCl_2$ and the number of moles of $CuCl_2$ are functions of time since they will change along with the hydrolysis reaction propagation. Therefore the volume and number of moles of $CuCl_2$ can be represented by equations 3.26 and 3.27, respectively.

$$V(t)_{CuCl_2} = n(t)_{CuCl_2} \times \frac{M_{CuCl_2}}{\rho_{CuCl_2}} \quad (3.26)$$

$$n(t)_{CuCl_2} = n_{CuCl_2,initial} - \frac{dn_s}{dt} t \quad (3.27)$$

The initial number of moles can be calculated by measuring the initial weight of $CuCl_2$.

$$n_{CuCl_2,initial} = \frac{m_{CuCl_2,initial}}{M_{CuCl_2}} \quad (3.28)$$

Considering Equation 3.20, the volume of CuCl_2 is redefined by Equation 3.29.

$$V(t)_{\text{CuCl}_2} = \frac{M_{\text{CuCl}_2}}{\rho_{\text{CuCl}_2}} \left(\frac{m_{\text{CuCl}_2, \text{initial}}}{M_{\text{CuCl}_2}} - \left| \frac{dn_{\text{HCl}}}{dt} \right| t \right) \quad (3.29)$$

The reaction rate of the hydrolysis reaction will be calculated by using equations 3.20, 3.26, and 3.29, respectively.

Chapter 4

Experimental Design

The experimental apparatus comprises the following main components: nitrogen tank, humidifier, preheater, reactor, and scrubber, as shown in 4.1. Here 316 Stainless steel pipes are used to connect the three different pipe sizes according to outer diameters of 1.0, 0.5, and 0.25 inches. The pipeline in a humidifier is supported by a bypass pipeline to control steam flow passing to the reactor. N_2 gas is passed through the pipes. The measurements are obtained from a flow control valve, pressure transducer, humidity sensor and six thermocouples. De-ionized water is poured into the pipes inside the humidifier using a two-way valve. The temperature of the humidifier is set to the desired value. Humidifier temperature controls the vapour flow. Water vapour is added to the flow in the humidifier. Both gases then pass and heat up through the preheater and reactor. The pipes are thermally insulated from the humidifier to the reactor. After the reactor, N_2 , product gas HCl, and unreacted H_2O are directed to pass through the NaOH solution in the scrubber for HCl to react and produce the salt NaCl.

4.1 Material Selection for the Apparatus

As the reaction products are corrosive-based gases, the material selection for the pipes and reactor was analyzed. Copper-based alloys could not be selected because pipe or reactor materials might react with gases, resulting in an error. The available other materials and their respective corrosive resistance against HCl and Cl_2 are shown in Table 4.1.

Hastelloy B is the first candidate for the pipes, followed by Hastelloy C. More sophisticated equipment was required to machine Hastelloy material. The cost of the material was essentially more expensive than other materials. Considering the other materials' corrosive resistance and supply parts' availability, 316 stainless

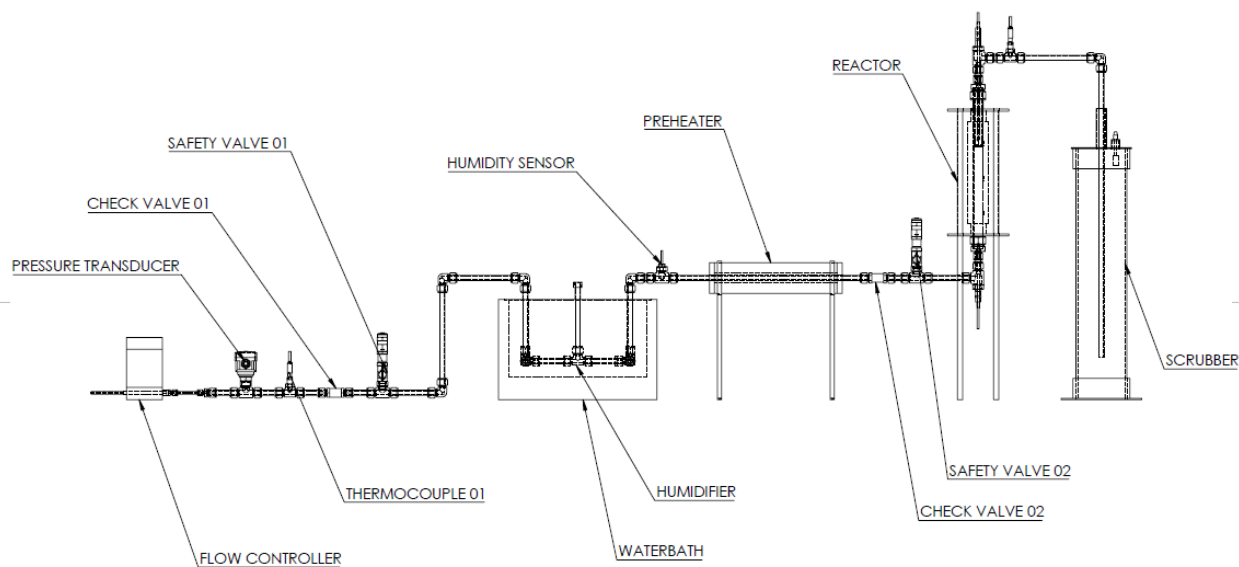


Figure 4.1: Schematic of the experimental design

steel was selected for the experiment. The reactor bed was manufactured with stainless steel. Coating inside the pipe with resisting materials increases the lifetime of parts. But a minimum internal diameter of 3.5 inches was required. The largest reactor pipe's external diameter was 1 inch.

4.2 Reactor and Reactor Bed Design

The cylindrical ceramic heater Omega CRFC-1512/120-C-A and Omega CRFC-112/120-C-A were used to heat the gases flowing inside the reactor pipe. The heater can achieve a high temperature of 982 °C. The reactor schematic is shown in Figure 4.2. Three thermocouples were fixed to read the inline temperature below / above the reactor bed and after the reactor. The reactor setup is connected to the system via two union sockets resulting in the ability to engage/disengage to modifications or new reactor setups.

The reactor bed must facilitate a place of the solid reactant, CuCl_2 and pass the reactant gas H_2O with carrier gas N_2 to flow. The bed was made of two annular plates holding a mesh in between to place the reactant. The bed was built with the same material as the pipe, 316 stainless steel. Maintaining a uniform temperature profile inside the reactor is crucial for readings. Thus the thickness of the bed was limited to 7mm. The bed needed to be positioned at the midpoint of the reactor pipe. Four supportive 1mm stands were utilized for positioning. The supports were installed upstream of the reactor bed to prevent contact with the supports and corrosive gases. The corrosive environment inside the reactor, four stands and the reactor bed were affected. Thus additional reactor beds were used. A schematic and actual bed are shown

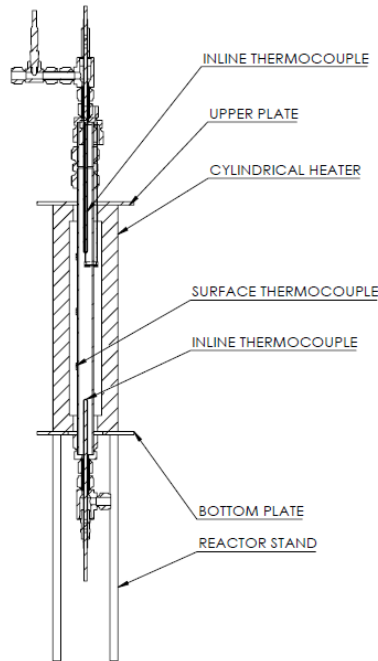


Figure 4.2: Hydrolysis reactor design

in Figure 4.3a and 4.3b, respectively.

Table 4.1: Corrosive resistance of materials

Material	HCl(aq), aerated	HCl(aq), air free	Cl ₂ (g)	Cl ₂ , wet
Carbon Steel	3	3	1	3
Cast Iron	3	3	1	3
Hastelloy B	1	1	1	1
Hastelloy C	2	2	1	1
304 and 304 Stainless Steel	3	3	1	1
316 Stainless Steel	3	3	1	1
416 Stainless Steel	3	3	1	1

1 - Good : 2 - Be Careful : 3 - Not usable

4.3 Pressure Drop of the Experimental Setup

The total pressure drop within the apparatus is the summation of the pressure drop due to the scrubber solution column, components, pipe friction, and fixed bed. The pressure drop for the scrubber solution can be represented by Equation 4.1.



(a) Schematic



(b) Fabricated reactor bed

Figure 4.3: Design and fabrication of the reactor bed

$$\Delta p_{Scrubber} = h_{immersed} \times \rho_{Scrubber} \times g \quad (4.1)$$

The NaOH solution is aqueous. The density of the scrubber solution is taken as the density of water at room temperature, 997 kg/m^3 [50]. The length of the pipe immersed in the scrubber is 64 cm. The predicted pressure drop of the scrubber is 6.260 Pa.

The temperature difference was used for to calculate pressure drops of components and frictional losses. The reactor and preheater units were designed at a temperature of $400 \text{ }^\circ\text{C}$. The remaining parts were considered to be room temperature. The volumetric flow rate was measured from the flow control valve. The flow was set to 1.00 SLM. The parameters of different diameter pipes are shown in Table 4.2. The same calculation process was used to determine the pressure drop of each pipe type. The carrier gas N_2 and steam are passed through the pipe configuration and NaOH solution column. The pressure drop inside the pipe was calculated by including major and minor losses.

Properties of gases passing through the system were calculated by assuming vapour contribution to the properties is negligible. The density of N_2 was calculated by Equation 3.12 using ideal gas conditions. The viscosity was measured from the graph of dynamic viscosity vs. temperature [51] at 1.0 bar. The Reynolds number was determined from Equation 4.2. The relative roughness could be determined according

Table 4.2: Parameters of experiments

Pipe Outer Diameter	1 inch	1/2 inch		1/4 inch	
Temperature (°C)	400	25	80	400	25
Pipe Length (m)	0.45	1.83	2.29	2.08	0.32
Density (kg/m ³)	0.0386	0.873	0.737	0.0386	0.0873
Dynamic Viscosity (μPas)	32	17	21	32	17
Flow Area (cm ²)	5.07	1.27	1.27	1.27	0.31
Velocity (m/s)	0.0337	0.1348	0.1348	0.1348	0.5395
Reynolds Number	41	346	237	82	693
Flow Type	laminar	laminar	laminar	laminar	laminar
Relative Roughness	0.000591	0.001181	0.001181	0.001181	0.002362
Friction Factor	1.570	0.185	0.270	0.785	0.092
Pressure Drop (Pa)	0.006	0.211	0.327	0.452	0.592

to Equation 4.3. The pipe was made of 316 stainless steel. The absolute roughness was noted as 0.015 mm [52]. The velocity in each section was calculated by using Equation 4.4. The friction factor was obtained from the Moody chart [53]. The corresponding pressure drop was derived according to Equation 4.5. The pressure drop due to the pipe friction is 1.6 Pa.

$$Re = \frac{\rho du}{\mu} \quad (4.2)$$

$$\text{Relative roughness} = \frac{\text{Absolute Pipe Roughness}}{\text{Pipe Diameter}} \quad (4.3)$$

$$\left(\rho_{N_2} \dot{V}_{N_2}\right)_{Initial} = \left(\rho_{N_2} u \times \frac{\pi d^2}{4}\right)_{Section} \quad (4.4)$$

$$\text{Friction factor} = \frac{2d}{\rho u^2 l} \times \Delta P \quad (4.5)$$

The pressure drop due to pipe components can be calculated from Equation 4.6. The components and respective resistance coefficients, K_i , are tabulated in Table 4.3. The total pressure drop of 3.2 Pa was obtained for component losses.

$$\Delta P = \sum K_i \frac{u^2}{2g} \quad (4.6)$$

Since the flow inside the reactor was determined to be laminar, the pressure drop of the fixed bed could be calculated from Ergun Equation 4.7 where ϵ , ϕ , and H are the porosity, sphericity, and height of the solid particles CuCl_2 , respectively. The porosity was taken as 0.17 from the literature [37]. The particles were observed to be tubular from SEM results, as shown in Figure 4.4. Therefore, the sphericity of the particles was calculated by using Equation 4.8 where a and b are the semi-major and semi-minor axes, respectively. Hence the pressure drop of the fixed bed was calculated to be 75.3 Pa so the pressure drop of the pipe system

Table 4.3: Pressure drop for component losses

Component	Quantity	K	Pressure Drop(Pa)
1/2" to 1/4" Reducing socket	2	0.6	0.193
1/2" T sockets	6	0.54	0.523
1/2" Elbow sockets	9	0.81	1.176
1/2" Three way valve	2	0.81	0.261
1/2" Union sockets	2	0.08	0.025
1/2" Check valve	2	2.7	0.871
1" to 1/2" reducing socket	2	0.6	0.193
1" Union sockets	2	0.08	0.001

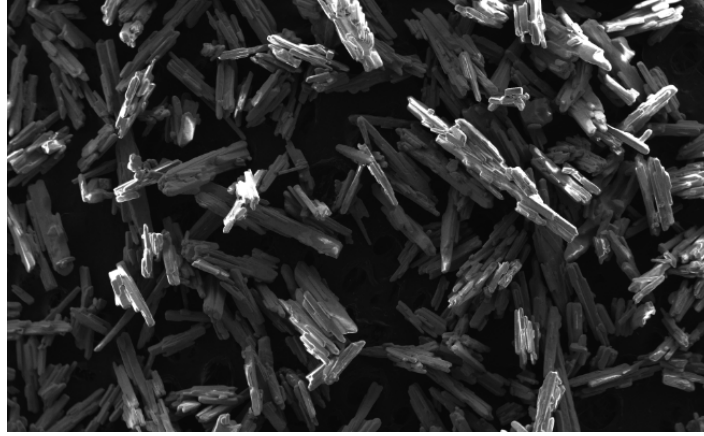


Figure 4.4: SEM images of solid reactant CuCl_2

was determined to be 6340.1 Pa.

$$-\frac{\Delta p}{H} = 180 \frac{\mu u (1 - \epsilon)^2}{\phi^2 d^2 \epsilon^2} \quad (4.7)$$

$$\phi = \frac{2 \sqrt[3]{ab^2}}{a + \frac{b^2}{\sqrt{a^2 - b^2}} \ln\left(\frac{a + \sqrt{a^2 - b^2}}{b}\right)} \quad (4.8)$$

4.4 Minimum Fluidization Velocity

The corresponding flow rate was compared with the minimum fluidization velocity of the solid reactant bed according to Equation 4.9 to ensure no pneumatic transport. The void fraction of the packed bed, which is the ratio between the void volume to the total volume of the packed bed, was taken as 0.17 [37]. The minimum fluidization velocity was determined as 0.340 m/s, which is higher than the operating velocity of the reactor bed. The fixed bed reactor design prevented pneumatic transport.

$$\text{Minimum Fluidization Velocity} = \frac{d^2 (\rho_p - \rho_g) g}{150 \mu} \frac{\epsilon \phi^2}{1 - \epsilon} \quad (4.9)$$

4.5 Safety and Risk Assessment

The carrier gas, N_2 , flows through the system. Within the humidifier, water vapour is added to the flow. Thereafter gaseous compounds will reach the reactor in which the hydrolysis reaction occurs. The product gas, HCl, remaining water vapour, and carrier gas, N_2 , flow into the scrubber. The scrubber is used to purify the gaseous compound. The HCl will react with NaOH to form NaCl. The hydrolysis reaction is represented by Equation 3.2.

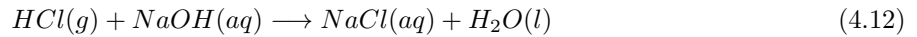
The initial $CuCl_2$ mass is taken as 5g. Therefore the initial amount of $CuCl_2$, N_{CuCl_2} , is

$$N_{CuCl_2} = \frac{m_{CuCl_2}}{M_{CuCl_2}} = \left(\frac{5g}{134.5g\text{mol}^{-1}} \right) = 0.03717 \text{ mol} \quad (4.10)$$

The amount of HCl after the complete conversion of $CuCl_2$, N_{HCl} is 0.03717 mol per the theoretical molar balance of the hydrolysis reaction 3.2. Assuming all Cl converts to HCl,

$$N_{HCl} = 2 \times N_{CuCl_2} = 0.74 \text{ mol} \quad (4.11)$$

The purifying reaction that occurs in the scrubber is shown by Equation 4.12.



Therefore, the required NaOH per experiment is 0.074 mol. The scrubber solution will contain twice this amount. The theoretically required NaOH amount is 0.148 mol. To ensure this level, an additional 5 percent of NaOH is added to the solution. The NaOH amount over 5 tests was 0.1554 mol.

A pH sensor was used to measure the acidity of the NaOH solution. The initial pH is 12. Therefore, the NaOH solution can be replaced when the pH value reaches 8. In the experiments, 10 litres of NaOH is used for the solution. The initial concentration of the NaOH solution is 0.01 molL^{-1} .

The minimum fluidization velocity for the $CuCl_2$ is $1.637 \times 10^{-6} \text{ ms}^{-1}$, and the corresponding volumetric rate is 4.00 LPM ($6.677 \times 10^{-5} \text{ m}^3\text{s}^{-1}$). The maximum temperature of the humidifier is $100 \text{ }^\circ\text{C}$. The water vapour density from the humidifier is 0.598 kgm^{-3} . At a relative humidity of 100 percent, the molar rate of water vapour is determined by Equation 3.13 to be $0.002218 \text{ mol s}^{-1}$.

The amount of HCl will be a maximum in the gas flow at stoichiometric conditions, according to the hydrolysis reaction on Equation 3.2 - twice the water vapour amount, 0.00443 mol^{-1} .

Inside the reactor, the maximum temperature is $400 \text{ }^\circ\text{C}$. The pressure is atmospheric pressure. Therefore

Table 4.4: Compound flow rates at the exit of the scrubber

Compound	Flow rate (m^3s^{-1})	Composition
N_2 +Excess Steam	6.677×10^{-5}	0.965
HCl(max)	2.449×10^{-6}	0.035

the volumetric flow rate of HCl can be calculated as $2.449 \times 10^{-4} \text{ m}^3 \text{ s}^{-1}$ from Equation 4.13.

$$\dot{V}_{HCl} = \frac{\dot{n}_{HCl}RT}{p} \quad (4.13)$$

The flow rates are tabulated in Table 4.4.

4.6 Temperature Controller and Electrical Design

The temperature profile inside the reactor is critical since isothermal conditions through the reactor are required. The temperature gradient, overshoot above the reference value, and differences between actual and reference values of the reactor temperature should be sensitively controlled. If not, undesirable reactions, such as the decomposition of CuCl_2 might occur. The temperature controller was used for both preheater and reactor ceramic heaters. The temperature controller is an Omega CN16D3-SR-2U-CM-AC which is utilized under the PID configuration, as shown in Figure 4.5. Both ceramic heaters are protected to the rated current of 5A. The heaters are powered by a relay Omega SSRL240DC10. Pulse Width Modulation signals are transmitted to the relays according to the difference between the reference value and the actual value.

The electrical components of the apparatus include the measuring system, heater system, and supportive equipment, as per Figure 4.5. The DAQ system and flow control valve are powered at 120V AC. The pressure transducer and humidity sensor are direct current. Direct current voltage supply was used to power them. The power supply was connected to 120V AC. For the heater system, there are two 120V AC connections for each ceramic heater for the temperature controller and the heater through the relay. Three other units - humidifier, heating tape, and fume extractor - were connected to 120V AC separately.

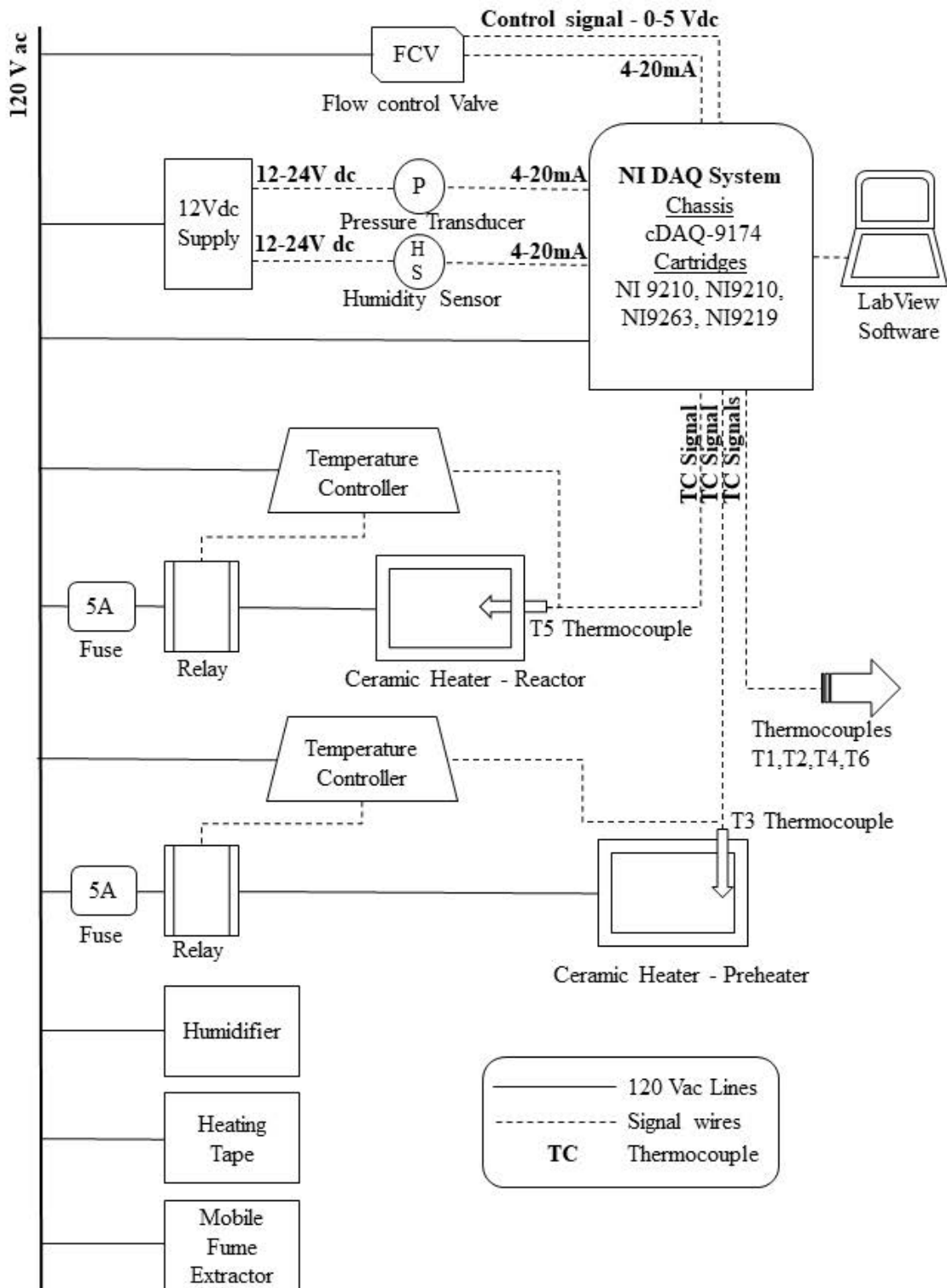


Figure 4.5: Electrical circuit of the experiment

Chapter 5

Experimental Measurements

5.1 DAQ System

The data acquisition system was completed by a National Instruments arrangement. The DAQ system was made of NI chassis cDAQ-9174, NI 9210, NI 9263, and NI 9219 cartridges. LabView software was used to produce the graphical user interface with NI DAQ assist. The total number of inputs and outputs were 09 and 01, respectively. The analog current input of 4 – 20 mA was received from the flow control valve, pressure transducer, and humidity sensor to the cartridge, NI 9219. The current input signals were proportional to the measurements. The range of the flow control valve, pressure transducer and humidity sensor was 0 – 10 SCCM, 0 – 2 bar, and 0 – 100 %, respectively. The analog current inputs were scaled and mapped with respect to their corresponding range. The flow control valve was directly powered by 120 V AC. Therefore, it was capable of transmitting analog signals without any additional modifications.

The pressure transducer and humidity sensor are connected to a 12-24 V DC power supply in series. To obtain accurate signals, a supporting resistor of $249\ \Omega$ must be connected in series. The six thermocouple readings were obtained from two NI 9210 cartridges. The initial temperature (T1) and final temperature (T2) were measured by type J Omega TC-J-NPT-G-72 thermocouples. The inline temperatures upstream of the reactor bed (T3) and after the reactor bed (T4) temperatures inside the reactor were measured by type T Omega XCIB-T-1-3-10 thermocouples. The inline thermocouples measure the temperature before and after the reactor bed. Both were protected with a probe to withstand the corrosive environment inside the reactor. The remaining thermocouples, type J Omega WTJ-6-60, measured surface temperatures (T2 and T3). The only output signal for the experimental setup was to control the flow rate of the flow control



Figure 5.1: Completed experimental setup

Table 5.1: Sensors and transducers used for the experiment

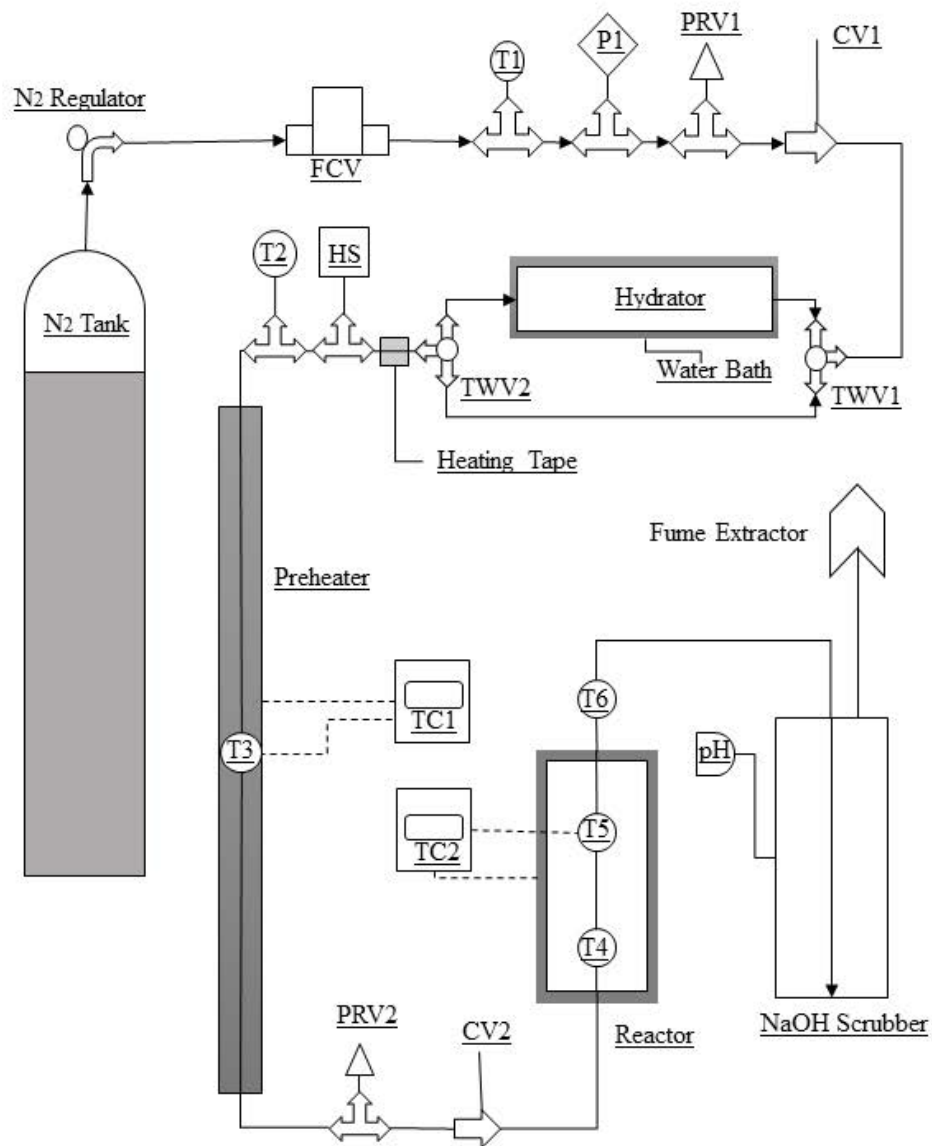
Parameter	Variable	Sensor/ Transducer	Accuracy
Flow rate	\dot{V}_{N_2}	Omega FMA-A2409 Flow Controller	± 0.01 SLM
Initial Pressure	P	Burkert 8311 - Pressure Transducer	± 0.01 bar
Initial Temperature/ Final Temperature	T1/ T6	Omega TC-J-NPT-G-72 Thermocouple	± 0.1 °C
Relative Humidity	HS	Omega HX200HR-W Humidity Transmitter	± 1.0 %
Humidifier Temperature/ Preheater Temperature	T2/ T3	Omega WTJ-6-60 Thermocouple	± 0.1 °C
Inline Temperatures	T4/ T5	Omega XCIB-T-1-3-10 Thermocouple	± 0.1 °C

valve. The flow control valve was controlled by a 0 - 5.0 V DC voltage signal which was produced by the NI cartridge 9263. The process flow diagram is shown in Figure 5.2. The final condition of the experimental setup is shown in Figure 5.1.

5.2 Calculation of Chloride Ions and pH Value

The software Lab View was used to measure the experimental variables. A time interval of 30 seconds was first used to extract a sample of 50 μ l from the NaOH solution. Then the experiment was operated for a total time of 30 minutes. After analyzing results, the time interval between extraction of samples and the total time was changed.

The undesired decomposition reaction which occurs during the hydrolysis reaction is shown as Equation 3.4. The NaOH scrubber is used to mitigate the possibility of toxic gases released to the surrounding area.



Abbreviation	Description	Abbreviation	Description
T	Temperature controller	TWV	Three-way valve
P	Pressure transducer	HS	Humidity Sensor
PRV	Pressure relief valve	TC	Temperature controller
CV	Control valve	pH	pH Sensor

Figure 5.2: Process flow diagram of the experiment

This considers the condition in which all CuCl_2 decomposes. The amount of $\text{Cl}_2(\text{g})$ released to the NaOH Scrubber, n_{Cl_2} , is given by

$$n_{\text{Cl}_2} = \frac{1}{2} \times n_{\text{CuCl}_2,i} \quad (5.1)$$

The Cl_2 gas reacts with the NaOH solution and results in NaCl, NaClO and H_2O as per Equation 5.2.



Therefore, the reacted NaOH mole quantity will be Δn_{NaOH} ,

$$\Delta n_{\text{NaOH}} = 2 \times n_{\text{Cl}_2} \quad (5.3)$$

The initial and final concentration of NaOH solution can be found from equations 5.4 and 5.5,

$$C_{i,\text{OH}^-} = 10^{14-\text{pH},i} \quad (5.4)$$

$$C_{f,\text{OH}^-} = 10^{14-\text{pH},f} \quad (5.5)$$

Considering the resolution of the pH meter, the pH change becomes:

$$\Delta \text{pH} = \text{pH}_f - \text{pH}_i = \lg \left(\frac{C_{\text{OH}^-,f}}{C_{\text{OH}^-,i}} \right) \quad (5.6)$$

The difference in the concentration levels can be expressed as,

$$C_{\text{OH}^-,f} = C_{\text{OH}^-,i} - \left(\frac{\Delta n_{\text{NaOH}}}{V} \right) \quad (5.7)$$

Here V, A, and H are the volume, cross-sectional area, and height of the scrubber solution, respectively.

$$V = A \times H \quad (5.8)$$

Therefore, the obtainable pH difference would be:

$$\Delta \text{pH} = \text{pH}_f - \text{pH}_i = \lg \left(\frac{C_{\text{OH}^-,i} - \left(\frac{\Delta n_{\text{NaOH}}}{V} \right)}{C_{\text{OH}^-,i}} \right) \quad (5.9)$$

This pH change should be detectable by the pH meter.

$$\Delta pH \geq \Delta pH_{resolution} \quad (5.10)$$

Thus,

$$C_{OH,i} \geq \frac{m_{CuCl_2}}{M_{CuCl_2} \times V} \times \left(\frac{1}{10^{\Delta pH_{resolution}}} \right) \quad (5.11)$$

The initial mass of $CuCl_2$ is 5 g and M_{CuCl_2} is 134.5 g/mol. The volume of the reactor is 5.5 L while the pH resolution is 0.01 for Omega PHH103B. Therefore, the initial NaOH molarity is 6.607×10^{-3} mol/L.

5.3 Uncertainty Analysis

An uncertainty analysis was carried out for the experimental results according to the method of Kline and McClintock. The bias and precision errors were calculated by considering sensitivities and measured results of the experiment at equilibrium conditions for 50 samples over a time interval of 20 s of sensors and transducers. The uncertainty, U_i was determined by Equation 5.12, where B_i and P_i represent the corresponding bias error and precision error of a sensor, respectively. The bias errors and precision errors are presented in Table 5.2. The propagation of uncertainties was determined by equations 5.12 to 5.19.

$$U_i = \sqrt{B_i^2 + P_i^2} \quad (5.12)$$

$$B^2_{\dot{n}_{N_2}} = \dot{n}_{N_2}^2 \left(\left(\frac{B_{T_1}}{T_1} \right)^2 + \left(\frac{B_P}{P} \right)^2 + \left(\frac{B_{\dot{V}_{N_2}}}{\dot{V}_{N_2}} \right)^2 \right) \quad (5.13)$$

$$B^2_{\dot{n}_{H_2O,in}} = \dot{n}_{H_2O,in}^2 \left(3 \left(\frac{B_{T_H}}{T_H} \right)^2 + \left(\frac{B_{RH}}{RH} \right)^2 + \left(\frac{B_{\dot{n}_{N_2}}}{\dot{n}_{N_2}} \right)^2 \right) \quad (5.14)$$

$$B^2_{\dot{n}_{HCl}} = \dot{n}_{HCl}^2 \left(2 \left(\frac{B_{m_{Cl^-}}}{m_{Cl^-}} \right)^2 + \left(\frac{B_t}{t} \right)^2 \right) \quad (5.15)$$

$$B^2_{\dot{r}_{CuCl_2}} = \dot{r}_{CuCl_2}^2 \left(\left(\frac{B_{m_{CuCl_2}}}{m_{CuCl_2}} \right)^2 + 2 \left(\frac{B_{\dot{n}_{HCl}}}{\dot{n}_{HCl}} \right)^2 \right) \quad (5.16)$$

$$P^2_{\dot{n}_{N_2}} = \dot{n}_{N_2}^2 \left(\left(\frac{P_{T_1}}{T_1} \right)^2 + \left(\frac{P_P}{P} \right)^2 + \left(\frac{P_{\dot{V}_{N_2}}}{\dot{V}_{N_2}} \right)^2 \right) \quad (5.17)$$

Table 5.2: Bias and precision errors associated with the measurement devices

Variable	Sensor/Transducer	Accuracy	Device range	Reference value	Relative bias error	Relative precision Error
\dot{V}_{N_2}	Omega FMA-2409 Flow Controller	± 0.01 SLM	0-10 SLM	1.0 SLM	0.01	0.000303
m_{Cl^-}	Geneq MKII chloride analyzer 926	± 3.0 mg/L	0-999 mg/L	233 mg/L	0.01287	5.165
HS	Omega HX200HR-W humidity transmitter	± 1.0 %	0-100 %	100 %	0.01	0.2234
$T2(T_H)$	Omega WTJ-6-60 Thermocouple	± 0.1 °C	0-480 °C	80 °C	0.00125	4.638
$T1$	Omega TC-J-NPT-G-72 thermocouple	± 0.1 °C	0-480 °C	25 °C	0.004	0.0337
V_p	Eppendorf Research plus pipette	± 2 μ L	500 μ L	500 μ L	0.004	-
t	Thomas Scientific stopwatch -HS43	-	86400 s	60 s	-	0.011
m_{CuCl_2}	Scale weight	± 0.001 g	0-999 g	5 g	0.0002	-
$T5$	Omega XCIB-T-1-3-10 thermocouple	± 0.1 °C	0-980 °C	400 °C	0.00025	0.5268
P	Burkert 8311 - pressure transducer	± 0.01 bar	0-2 bar	0.12 bar	0.083	30.30
pH	Omega PHH-103A pH meter	± 0.02 pH	0-14 pH	14 pH	0.0014	-

Table 5.3: Propagation of experimental uncertainty

Variable	Equations	Bias Error	Precision Error	Uncertainty
\dot{n}_{N_2}	5.13 and 5.17	0.0100	0.0031	0.0105
\dot{n}_{H_2O}	5.14 and 5.18	0.0735	0.0229	0.0077
\dot{n}_{HCl}	5.15 and 5.20	0.0001	0.00035	0.0004
\dot{r}_{CuCl_2}	5.16 and 5.19	0.0002	0.3005	0.3005

$$P^2_{\dot{n}_{H_2O, in}} = \dot{n}_{H_2O, in}^2 \left(3 \left(\frac{P_{T_H}}{T_H} \right)^2 + \left(\frac{P_{RH}}{RH} \right)^2 + \left(\frac{P_{\dot{n}_{N_2}}}{\dot{n}_{N_2}} \right)^2 \right) \quad (5.18)$$

$$P^2_{\dot{n}_{HCl}} = \dot{n}_{HCl}^2 \left(2 \left(\frac{P_{m_{Cl^-}}}{m_{Cl^-}} \right)^2 + \left(\frac{P_t}{t} \right)^2 \right) \quad (5.19)$$

$$P^2_{\dot{r}_{CuCl_2}} = \dot{r}_{CuCl_2}^2 \left(\left(\frac{P_{m_{Cl^-}}}{m_{Cl^-}} \right)^2 + 2 \left(\frac{P_{\dot{n}_{HCl}}}{\dot{n}_{HCl}} \right)^2 \right) \quad (5.20)$$

The calculated values are presented in Table 5.3. The overall measurement uncertainty of the experiments was determined to be 30.1%.

Chapter 6

Results and Discussion

6.1 Analysis of Reactor Outputs

The reactor bed solid compounds were investigated to identify available solid products and remaining reactants. The solid reactant, hydrated CuCl_2 , anhydrous CuCl_2 and product Cu_2OCl_2 , are shown in figures 6.1a, 6.1b, and 6.1c, respectively. The 5 g of heated anhydrous CuCl_2 was placed on the reactor bed for one run. Once the experimentation was completed, the apparatus was set to cool down overnight to room temperature. The humidifier was bypassed to ensure any additional steam entered the reactor. The carrier gas, N_2 , was flown until the relative humidity sensor reached 0% to confirm that the available steam exited the apparatus. Thereafter, cooled solid products were examined by an XRD machine. Unfortunately, XRD demonstrated an unusual background and low diffraction peaks, indicating that the sample was either not crystalline or had contained other compounds that were not crystalline. Therefore, available compounds could not be identified with certainty. An XRD analysis was performed for two product samples and 15 reactant samples which included dried, hydrated and crushed samples, although the same issues occurred.

The reaction extent was quantified by the gaseous output. Unlike the solid compound investigation, gaseous products were not directly measured. They passed through the scrubber solution, and the calculation used prior models in Chapter 3. The change in the chlorides per minute was measured by a Geneq MKII chloride analyzer 926. The experimentation provided reasonable values that will be discussed later in this chapter. The reaction kinetics and other results were obtained from the gaseous output data.

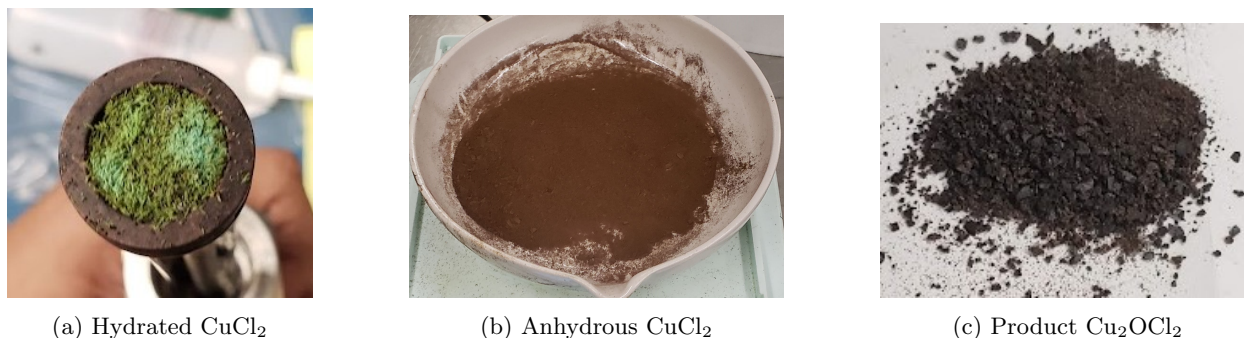


Figure 6.1: Solid samples of reactants and products

6.2 Partial Pressure and Molar Fraction of Steam

The partial pressure of steam was investigated with the reaction kinetics of the hydrolysis reaction. The reaction extent and reaction rate were analyzed with respect to the above properties of steam. The molar fraction was determined according to Equation 6.1. The partial pressure and molar fraction of steam are presented in Figure 6.2. Both pressures gradually increased with time because of the pressure drop through the reactor bed while changing with products and reactants. Throughout each test, the molar fraction and partial pressure showed stable behaviour.

$$y_{H_2O} = \frac{p_{H_2O}}{p} \quad (6.1)$$

From the measured results, the reaction extent and the reaction rate of the hydrolysis reaction do not appear to have a direct relationship with the steam pressure and molar fraction.

6.3 Order of Irreversible Hydrolysis Reaction

As described in Chapter 3, the hydrolysis reaction is modelled by two separate approaches as reversible equilibrium reaction and an irreversible first-order reaction. The studies were unable to achieve equilibrium for the test. Trends can be seen in the graph of the conversion of CuCl_2 vs. time presented in Figure 6.4. The order of the hydrolysis reaction was calculated from Equation 6.3. The gradient of the results of Equation 6.3 must be equal to the order of the reaction, while the reaction rate constant can be obtained by the intercept. The graph is presented in Figure 6.3. The equation of the line was calculated to be $y = 0.832x - 1.6012$. The slope of the graph is 0.832. The order of the hydrolysis reaction was determined to be a first-order reaction.

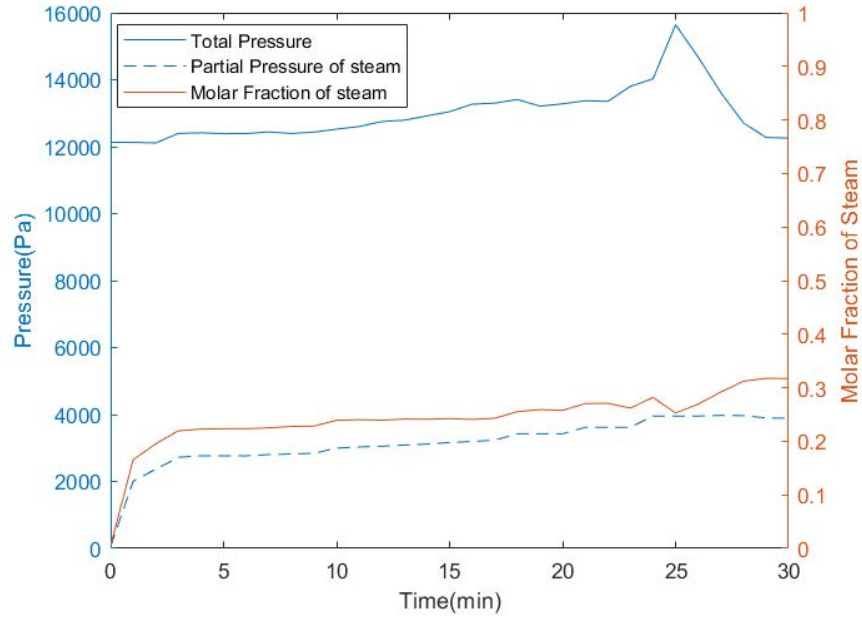


Figure 6.2: Partial pressure and molar fraction of steam over time

$$\dot{r}_{CuCl_2} = kC_{H_2O}^n \quad (6.2)$$

$$\ln(\dot{r}_{CuCl_2}) = n \times \ln(C_{H_2O}) + \ln(k) \quad (6.3)$$

6.4 Thermophysical Properties

The experiment was performed at 390 °C for 30 minutes. The measured conversion over time is shown in Figure 6.4. The measured results were compared with experimental data of conversion in the hydrolysis reaction at 375 °C by Ferrandon et al. [54] for particles of 100 µm radius. Argon was taken as the carrier gas. Discrepancies between the results were due to changes in the reaction temperature, particle size, initial solid reactant mass, carrier gas and reactor configuration.

The rate of conversion increased like a linear function. The total time for complete conversion was taken as 42.8 min. The vapour pressure was calculated from Equation 6.4. As demonstrated in Figure 6.3, the intercept of the graph leads to the reaction rate coefficient, which was determined as 0.201 65 s⁻¹.

$$P_{H_2O} = RH \times P_{sat} \quad (6.4)$$

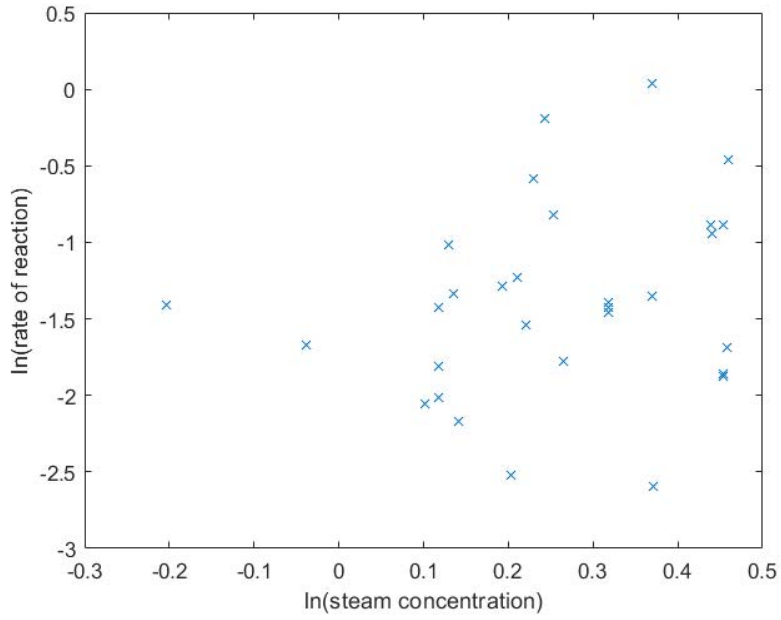


Figure 6.3: Order of hydrolysis reaction

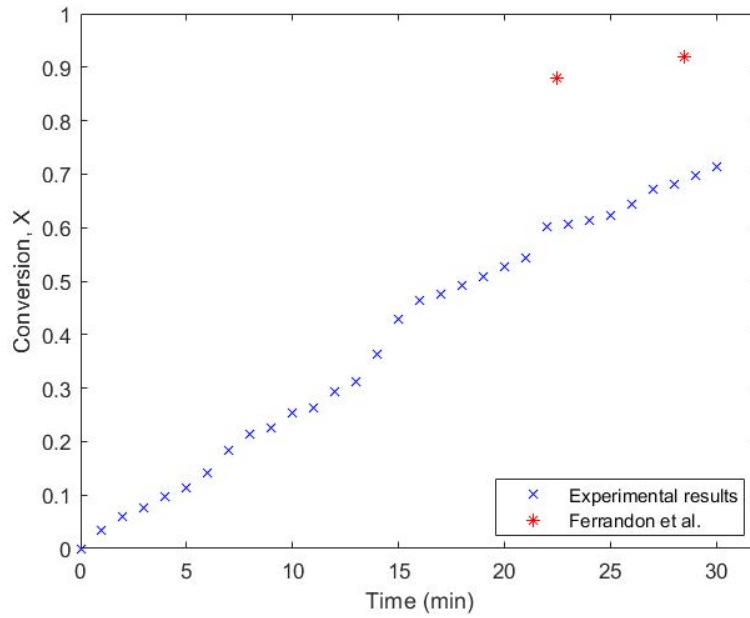


Figure 6.4: Conversion of hydrolysis reaction over time

The density of steam was determined based on Equation 3.10. Once the humidifier pipeline was included in the system, the relative humidity of the pipe became 100%. The humidifier temperature was gradually increased. The density of steam and the reactor temperature was analyzed and compared with past values in the literature. The behaviour is presented in Figure 6.5. The average density of steam was 10.52 g/m^3 . Past literature used a density of steam of 17 g/m^3 in a vertical reactor at $390 \text{ }^\circ\text{C}$ over an experiment of 30 minutes [45].

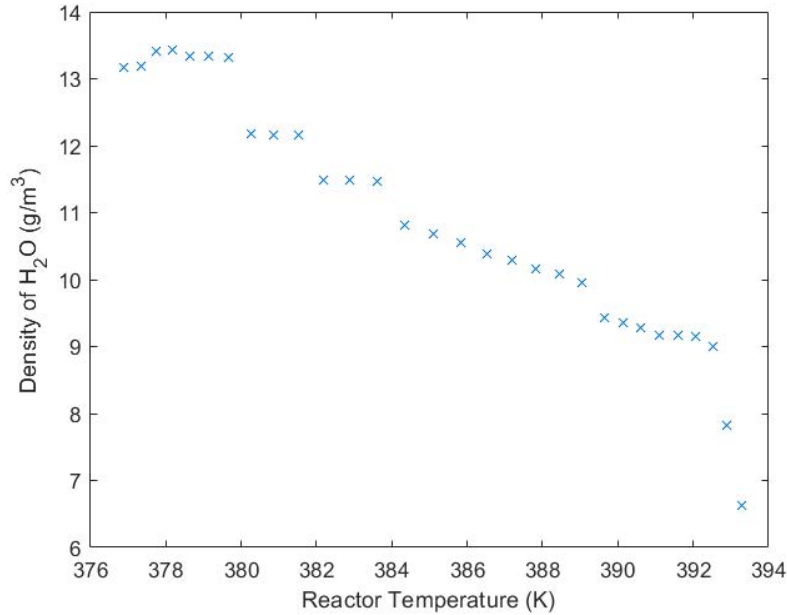


Figure 6.5: Density of H₂O vs. reactor temperature

6.5 Controlling Resistance

The conversion vs. (t/τ) was determined from experimental results and two major resistances as denoted in equations 3.24 and 3.23, respectively. The graphs are shown in Figure 6.6. The experimental results demonstrated a trend to follow the pattern of surface reaction resistance than that of diffusion resistance, according to the graph. The R squared values for two resistances to mass transfer considered the experimental reaction being controlled by diffusion and surface reaction are -0.889 and 0.879 , according to equations 3.21 and 3.22. Hence, the calculated R squared value confirmed the resistance step of the reaction regarding the experiment for surface reaction control. The sphericity was 0.6795 and the average diameter was $619 \mu\text{m}$ for the sample. The hydraulic diameter was determined to be $421 \mu\text{m}$. Therefore, the controlling resistance for spherical particles of an initial diameter of $421 \mu\text{m}$ was found to be the surface reaction resistance.

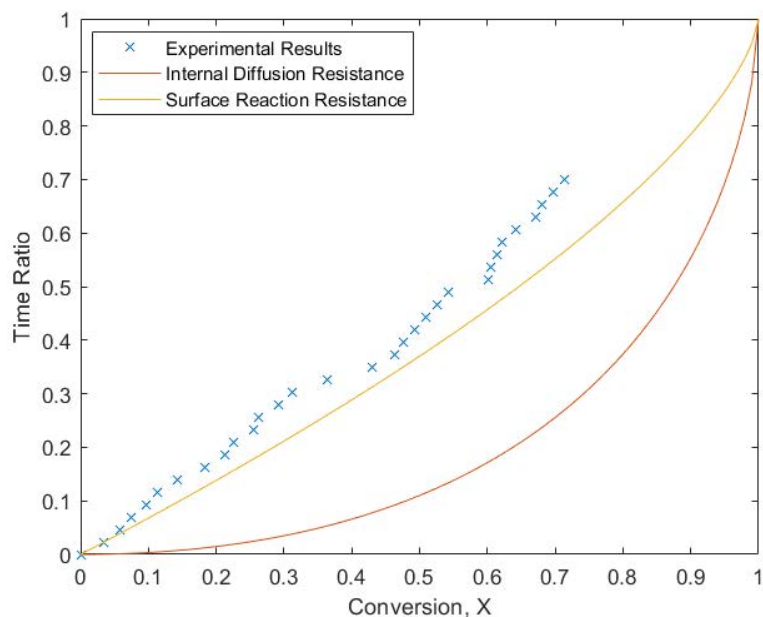


Figure 6.6: Time ratio of hydrolysis reaction vs. conversion

6.6 Reaction Rate of Hydrolysis Reaction

For the duration of 30 minutes of the experiment, the reaction rate fluctuated between $5.14 \times 10^{-3} \text{ mol/cm}^3\text{min}$ and $1.46 \times 10^{-3} \text{ mol/cm}^3\text{min}$. The temperature inside the reactor was maintained at 390°C . The reaction

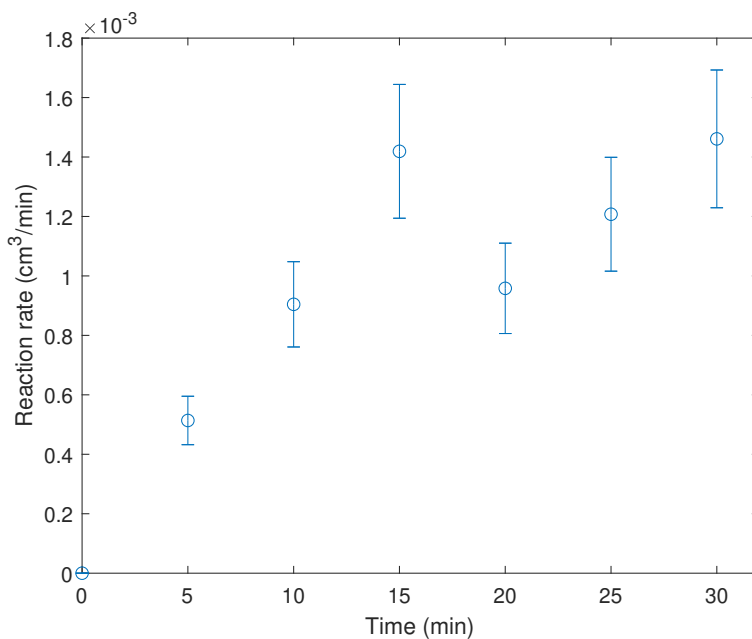


Figure 6.7: CuCl_2 hydrolysis reaction rate over time

rate increased to 1.42×10^{-3} mol/cm³min for 15 minutes. The packed bed was filled by solid reactants. The heated N₂ and steam passed through the center of the mesh. The previous experiments showed that solid reactants placed in the center reacted first. After 15 minutes, the solid reactant on the center had reacted completely, forcing steam to react with the CuCl₂ near the perimeter of the mesh.

In Figure 6.2, the total pressure is gradually increasing. The change of pressure at any instant and the initial pressure accounted for any difference that occurred in the fixed bed since the remaining items of the apparatus weren't changed. The gradual increase of pressure could be explained as the newly produced product layer, Cu₂OCl₂ was filling the void of the packed bed in the center. Gases passed through different paths away from the center resulting in gas flow through the unreacted solid reactants at the edge of the mesh. This created a similar condition to the solid reactants in the center of the mesh. The reaction rate was again gradually increasing.

Chapter 7

Conclusions and Recommendations

7.1 Conclusions

In this research, the reaction kinetics of the hydrolysis reaction of the Cu-Cl cycle was investigated through experimental studies. An experimental setup was designed and fabricated to operate at atmospheric pressure and a temperature of 390 °C. As a heterogeneous reaction, hydrolysis of CuCl_2 with water vapour showed its characteristics of resistance to mass transfer in three ways: external diffusion resistance, internal diffusion resistance and reaction surface resistance. The controlling resistance step with respect to initial particle size was analyzed.

The key findings of the research were experimental values for thermophysical property. The measured reaction rate coefficient is 0.20165 s^{-1} . The particle diameter of the sample was $620 \mu\text{m}$, and the sphericity was 0.6795.

This sample exhibited a surface reaction resistance as the controlling step. According to the shrinking core model and heterogeneous reaction concepts, the particles smaller than the effective particle size should exhibit internal diffusion resistance to be the controlling step. According to Figure 6.6 and R squared values, the results indicated that the controlling resistance of the experimental study is a surface reaction for a particle size having a hydraulic diameter of $421 \mu\text{m}$. In future studies, an experimental test should be performed longer than the complete conversion time. For this sample, a minimum duration of the experiment of longer than 42.8 min is recommended.

A range of particle sizes is recommended in future studies for the same operational condition. The controlling resistance must be determined by the R squared value and Figure 6.6. The measured results showed that an effective particle size is available and that the diameter is larger than a hydraulic diameter of 421 μm . When the controlling resistance is found to be internal diffusion, then the run time for complete conversion should be used based on Equation 3.24.

The analysis of solid products assists in validating and understanding the hydrolysis reaction inside the reactor. The XRD analysis must be performed with higher accuracy. The measured results were unable to clearly identify the XRD patterns due to the lack of crystalline material in the sample. The available compounds of solid products indicate the possibility of undesirable reactions including the thermal decomposition of CuCl_2 and Cu_2OCl_2 . Past literature showed that apart from the expected product, Cu_2OCl_2 , the compounds of CuO and CuCl were present in the products. A set of 12 experimental tests ranged from 5 minutes to 60 minutes, increasing by 5 minutes, is recommended in future studies for the same operating conditions of temperature and pressure. All samples should have an XRD analysis and mass balance. A relative compound ratio can be obtained from XRD analysis and compared with results for validation.

The selected material, stainless steel 316, for the pipe system of the experiment was used in the design. Due to the corrosiveness of HCl gas, the piping and reactor were affected. The inside surface of the pipe was constantly cleaned to prevent any undesirable compounds in the byproducts. Another suitable candidate for the pipe material is Hastelloy B as determined by Table 4.1. Implementation of Hastelloy B is recommended in future studies.

7.2 Recommendations

The incoming rate of water vapour to the reactor is measured using a humidity sensor installed between the preheater and humidifier. After the reactor, HCl gas also accompanies it. HCl gas produces a corrosive environment that prevents another humidity sensor after the reactor. Inline measurement of the rate of water vapour exiting the reactor is expected to provide more accurate results. Installation of a humidity sensor that can withstand corrosive gases after the reactor is recommended.

The possibility of undesirable side reactions occurring with hydrolysis reaction was minimized by maintaining the optimum operating temperature within the reactor. The most probable side reaction is the decomposition of solid reactant CuCl_2 . Since one of the products is Cl_2 , the reacted amount could be deter-

mined using the amount of Cl_2 in the scrubber solution. The pH value and chloride amount are measured in the scrubber. The Cl_2 gas has relatively low solubility in the NaOH aqueous solution. Therefore, installing a sensor to read the Cl_2 rate before the scrubber solution is recommended.

The reactor bed was designed to place the solid reactant CuCl_2 . The flow rate is controlled at less than the minimum fluidization velocity. Nevertheless, there could be possible ways to increase pressure which later pneumatically transports solid particles placed on the reactor bed. To prevent the velocity increasing above the minimum fluidization velocity, two mesh lids should be added to the reactor bed from both the top and bottom in future studies.

Due to the high temperature inside the reactor, CuCl_2 vapour might form and pass to the scrubber solution. The chloride ions of CuCl_2 are accounted in the final chloride measurement, which affects accuracy of measured values. Installing a sensor to measure the Cu amount or a chemical titration method to measure the Cu amount at regular intervals is recommended in future studies.

The procedure of inserting solid reactant material into the reaction bed and extracting solid products was found to be cumbersome due to the assembly and disassembly of parts, as described in the safety manual in Appendix A. The reason for the design was to use the cylindrical ceramic heater for the reactor. The cylindrical ceramic heater supplied a uniform temperature profile. But it did not allow for accurate material placement. A split-type furnace is recommended for the heater as it would facilitate direct access to the reactor bed through the pipe, unlike to current method in which pipe ends are used. The current heater has the induction wires placed on the inside wall of the heater, as shown in Figure 4.2. These conductive wires prevent any measuring equipment from reaching outside of the reactor pipe because there is a risk of a short circuit which will damage the heater and experimental setup.

The reaction kinetics of the hydrolysis reaction is an active research area. The measured results suggest that future research on the following cases will improve the knowledge of the reaction kinetics of the Cu-Cl thermochemical cycle.

- Case 01: Investigation of the controlling resistance vs mass transfer for the hydrolysis reaction for a range of particle sizes to locate the effective particle size and then validate experimentally.
- Case 02: Experimentation of effective particle size variations with respect to reaction temperature and pressure and to identify the effective particle size relationship against two properties.

- Case 03: Determining a relationship for thermophysical properties of the reaction rate coefficient and internal diffusion coefficient with respect to reaction temperature and pressure, and then experimentally validated.

Bibliography

- [1] Magali S Ferrandon, Michele A Lewis, David F Tatterson, Adam Gross, Denis Doizi, L Croize, V Dauvois, JL Roujou, Y Zanella, and P Carles. Hydrogen production by the cu-cl thermochemical cycle: Investigation of the key step of hydrolysing cucl₂ to cu₂ocl₂ and hcl using a spray reactor. *International Journal of Hydrogen Energy*, 35(3):992–1000, 2010.
- [2] VN Daggupati, GF Naterer, KS Gabriel, RJ Gravelins, and ZL Wang. Equilibrium conversion in cu-cl cycle multiphase processes of hydrogen production. *Thermochimica Acta*, 496(1-2):117–123, 2009.
- [3] Maan Al-Zareer, Ibrahim Dincer, and Marc A Rosen. Analysis and assessment of the integrated generation iv gas-cooled fast nuclear reactor and copper-chlorine cycle for hydrogen and electricity production. *Energy Conversion and Management*, 205:112387, 2020.
- [4] Marc A Rosen. Advances in hydrogen production by thermochemical water decomposition: a review. *Energy*, 35(2):1068–1076, 2010.
- [5] Rajendra V Singh, Mrinal R Pai, Atindra M Banerjee, Geeta R Patkare, Rajesh V Pai, Asheesh Kumar, Ashok K Yadav, Suhas Phaphale, and Arvind K Tripathi. Investigations on the hydrolysis step of copper-chlorine thermochemical cycle for hydrogen production. *International Journal of Energy Research*, 44(4):2845–2863, 2020.
- [6] Ryan J Andress, Xinqun Huang, B Wayne Bequette, and Lealon L Martin. A systematic methodology for the evaluation of alternative thermochemical cycles for hydrogen production. *International journal of hydrogen energy*, 34(9):4146–4154, 2009.
- [7] VN Daggupati, GF Naterer, KS Gabriel, RJ Gravelins, and ZL Wang. Solid particle decomposition and hydrolysis reaction kinetics in cu-cl thermochemical hydrogen production. *International journal of hydrogen energy*, 35(10):4877–4882, 2010.

- [8] Deepa Thomas, Neetu A Baveja, KT Shenoy, and JB Joshi. Mechanistic and kinetic study of thermolysis reaction with hydrolysis step products in cu-cl thermochemical cycle. *International Journal of Hydrogen Energy*, 46(24):12672–12681, 2021.
- [9] GD Marin, Z Wang, GF Naterer, and K Gabriel. X-ray diffraction study of multiphase reverse reaction with molten cucl and oxygen. *Thermochimica acta*, 524(1-2):109–116, 2011.
- [10] GF Naterer, S Suppiah, L Stolberg, M Lewis, S Ahmed, Z Wang, MA Rosen, I Dincer, K Gabriel, E Secnik, et al. Progress of international program on hydrogen production with the copperechlorine cycle. *international journal of hydrogen energy*, 39(2431):e2445, 2014.
- [11] VN Daggupati, GF Naterer, and KS Gabriel. Diffusion of gaseous products through a particle surface layer in a fluidized bed reactor. *International journal of heat and mass transfer*, 53(11-12):2449–2458, 2010.
- [12] Octave Levenspiel. *Chemical reaction engineering*. John wiley & sons, 1998.
- [13] Magali S Ferrandon, Michele A Lewis, Francisco Alvarez, and Evgeny Shafirovich. Hydrolysis of cucl₂ in the cu-cl thermochemical cycle for hydrogen production: experimental studies using a spray reactor with an ultrasonic atomizer. *international journal of hydrogen energy*, 35(5):1895–1904, 2010.
- [14] Stéphane Abanades, Patrice Charvin, Gilles Flamant, and Pierre Neveu. Screening of water-splitting thermochemical cycles potentially attractive for hydrogen production by concentrated solar energy. *Energy*, 31(14):2805–2822, 2006.
- [15] Shinji Kubo, Hayato Nakajima, Seiji Kasahara, Syunichi Higashi, Tomoo Masaki, Hiroyoshi Abe, and Kaoru Onuki. A demonstration study on a closed-cycle hydrogen production by the thermochemical water-splitting iodine-sulfur process. *Nuclear Engineering and Design*, 233(1-3):347–354, 2004.
- [16] Wei Wu, Fu Teng Hsu, and Han Yu Chen. Design and energy evaluation of a stand-alone copper-chlorine (cu-cl) thermochemical cycle system for trigeneration of electricity, hydrogen, and oxygen. *International Journal of Energy Research*, 42(2):830–842, 2018.
- [17] Rami S El-Emam, Hasan Ozcan, and Calin Zamfirescu. Updates on promising thermochemical cycles for clean hydrogen production using nuclear energy. *Journal of Cleaner Production*, 262:121424, 2020.
- [18] A Odukoya and GF Naterer. Upgrading waste heat from a cement plant for thermochemical hydrogen production. *International journal of hydrogen energy*, 39(36):20898–20906, 2014.

- [19] Aida Farsi, Ibrahim Dincer, and Greg F Naterer. Multi-objective optimization of an experimental integrated thermochemical cycle of hydrogen production with an artificial neural network. *International Journal of Hydrogen Energy*, 45(46):24355–24369, 2020.
- [20] GF Naterer, S Suppiah, L Stolberg, M Lewis, M Ferrandon, Z Wang, I Dincer, K Gabriel, MA Rosen, E Secnik, et al. Clean hydrogen production with the cu–cl cycle—progress of international consortium, i: experimental unit operations. *International Journal of Hydrogen Energy*, 36(24):15472–15485, 2011.
- [21] S Aghahosseini, I Dincer, and GF Naterer. Process integration of hydrolysis and electrolysis processes in the cu–cl cycle of hydrogen production. *International journal of hydrogen energy*, 38(23):9633–9643, 2013.
- [22] Faran Razi, Ibrahim Dincer, and Kamiel Gabriel. Thermal management of a new integrated copper-chlorine cycle for hydrogen production. *Energy Conversion and Management*, 212:112629, 2020.
- [23] Hoseyn Sayyaadi and Milad Saeedi Boroujeni. Conceptual design, process integration, and optimization of a solar cucl thermochemical hydrogen production plant. *International Journal of Hydrogen Energy*, 42(5):2771–2789, 2017.
- [24] S Aghahosseini, I Dincer, and GF Naterer. Linear sweep voltammetry measurements and factorial design model of hydrogen production by hcl/cucl electrolysis. *International journal of hydrogen energy*, 38(29):12704–12717, 2013.
- [25] Samane Ghandehariun, Zhaolin Wang, Marc A Rosen, and Greg F Naterer. Reduction of hazards from copper (i) chloride in a cu–cl thermochemical hydrogen production plant. *Journal of hazardous materials*, 229:48–56, 2012.
- [26] Mehdi Mehrpooya and Roghayeh Habibi. A review on hydrogen production thermochemical water-splitting cycles. *Journal of Cleaner Production*, 275:123836, 2020.
- [27] Bharanidharan Rajasekaran and Ofelia A Jianu. Analytical prediction of heat capacity of molten agcl and cucl with application to thermochemical cu-cl cycle for hydrogen production. *International Journal of Hydrogen Energy*, 46(2):1583–1591, 2021.
- [28] O Jaber, GF Naterer, and I Dincer. Heat recovery from molten cucl in the cu–cl cycle of hydrogen production. *International Journal of Hydrogen Energy*, 35(12):6140–6151, 2010.
- [29] Tahir Abdul Hussain Ratlamwala and Ibrahim Dincer. Energy and exergy analyses of hybrid photocatalytic hydrogen production reactor for cucl cycle. *International Journal of Hydrogen Energy*, 43(9):4167–4176, 2018.

- [30] Yarkin Gevez and Ibrahim Dincer. Investigation of a new integrated energy system with thermochemical hydrogen production cycle and desalination. *Applied Thermal Engineering*, 203:117842, 2022.
- [31] MH Bölükdemir, H Koç, and E Eser. Calculation of thermophysical properties of copper compounds in cucl production cycle. *Journal of Physics and Chemistry of Solids*, 112:258–261, 2018.
- [32] Mudit Nijhawan, Geoffrey Ruytenbeek, Ofelia A Jianu, and Brian M Ikeda. Experimental process for material testing in molten salt environments for hydrogen production processes. *International Journal of Hydrogen Energy*, 47(10):6535–6543, 2022.
- [33] Wei Wu, Han Yu Chen, and Felicia Wijayanti. Economic evaluation of a kinetic-based copperchlorine (cucl) thermochemical cycle plant. *International Journal of Hydrogen Energy*, 41(38):16604–16612, 2016.
- [34] Şulenur Asal and Adem Acir. Utilization of the cu–cl thermochemical cycle for hydrogen production using a laser driver thorium molten salts. *International Journal of Hydrogen Energy*, 46(61):31133–31142, 2021.
- [35] Tomasz Wajda and Kamiel Gabriel. Thermolysis reactor scale-up for pilot scale cucl hybrid hydrogen production. *International Journal of Hydrogen Energy*, 44(20):9779–9790, 2019.
- [36] Wei Wu, Han Yu Chen, and Jenn-Jiang Hwang. Energy analysis of a class of copper–chlorine (cu–cl) thermochemical cycles. *International Journal of Hydrogen Energy*, 42(25):15990–16002, 2017.
- [37] K Pope, GF Naterer, and Z Wang. Pressure drop of packed bed vertical flow for multiphase hydrogen production. *International journal of hydrogen energy*, 36(17):11338–11344, 2011.
- [38] Leyla Ozgener, Arif Hepbasli, and Ibrahim Dincer. Energy and exergy analysis of geothermal district heating systems: an application. *Building and Environment*, 40(10):1309–1322, 2005.
- [39] Aida Farsi, Ibrahim Dincer, and Greg F Naterer. Second law analysis of cucl₂ hydrolysis reaction in the cu–cl thermochemical cycle of hydrogen production. *Energy*, 202:117721, 2020.
- [40] BCR Ewan and RWK Allen. Limiting thermodynamic efficiencies of thermochemical cycles used for hydrogen generation. *Green Chemistry*, 8(11):988–994, 2006.
- [41] K Kawashima, H Okabe, K Suzuki, S Kuroiwa, J Akimitsu, KH Sato, A Koda, and R Kadono. Anti-ferromagnetic ordering in cu₂ocl₂ studied by the muon spin rotation/relaxation technique. *Journal of Physics: Condensed Matter*, 19(14):145275, 2007.

- [42] Mehmet F Orhan, Ibrahim Dincer, and Marc A Rosen. Design of systems for hydrogen production based on the cu-cl thermochemical water decomposition cycle: configurations and performance. *international journal of hydrogen energy*, 36(17):11309–11320, 2011.
- [43] Maan Al-Zareer, Ibrahim Dincer, and Marc A Rosen. Development and assessment of a novel integrated nuclear plant for electricity and hydrogen production. *Energy Conversion and Management*, 134:221–234, 2017.
- [44] C Zamfirescu, I Dincer, and GF Naterer. Thermophysical properties of copper compounds in copper-chlorine thermochemical water splitting cycles. *International Journal of Hydrogen Energy*, 35(10):4839–4852, 2010.
- [45] K Pope, GF Naterer, and ZL Wang. Steam flow effects on hydrolysis reaction kinetics in the cu-cl cycle. *International journal of hydrogen energy*, 37(23):17701–17708, 2012.
- [46] Kamiel Gabriel, Leonard Finney, and Patrick Dolloso. Preliminary results of the integrated hydrolysis reactor in the cu-cl hydrogen production cycle. *international journal of hydrogen energy*, 44(20):9743–9752, 2019.
- [47] K Pope, GF Naterer, and ZL Wang. Nitrogen carrier gas flow for reduced steam requirements of water splitting in a packed bed hydrolysis reactor. *Experimental thermal and fluid science*, 44:815–824, 2013.
- [48] H Ishaq and I Dincer. A comparative evaluation of three cucl cycles for hydrogen production. *International Journal of Hydrogen Energy*, 44(16):7958–7968, 2019.
- [49] Kevin Pope, Zhaolin L Wang, and Greg F Naterer. Measured steam conversion and chemical kinetics in a hydrolysis packed bed reactor for hydrogen production. *Energy Procedia*, 29:496–502, 2012.
- [50] PROPERTY TABLES AND CHARTS (SI UNITS). https://homepages.wmich.edu/~cho/ME432/Appendix1Updated_metric.pdf. [Online; accessed 02- Aug- 2022].
- [51] Nitrogen - Dynamic and Kinematic Viscosity vs. Temperature and Pressure. https://www.engineeringtoolbox.com/nitrogen-N2-dynamic-kinematic-viscosity-temperature-pressure-d_2067.html. [Online; accessed 02- Aug- 2022].
- [52] Absolute Pipe Roughness. <https://www.enggcyclopedia.com/2011/09/absolute-roughness/>. [Online; accessed 02- Aug- 2022].
- [53] How to read a moody chart. <https://owlcation.com/stem/How-To-Read-a-Moody-Chart>. [Online; accessed 02- Aug- 2022].

- [54] Magali S Ferrandon, MA Lewis, David F Tatterson, Rohit V Nankani, M Kumar, LE Wedgewood, and LC Nitsche. The hybrid cu-cl thermochemical cycle. i. conceptual process design and h₂a cost analysis. ii. limiting the formation of cucl during hydrolysis. In *NHA annual hydrogen conference, Sacramento convention center, CA*, volume 10, pages 3310–3326, 2008.

Appendix A - Hydrolysis Reactor

Safety and Operations Manual

Introduction

In this research, experimental data is collected from a chemical reactor fabricated for the investigation of reaction kinetics in CuCl_2 hydrolysis. A hydrolysis reaction in which steam and CuCl_2 are reactants and HCl and Cu_2OCl_2 are products will be conducted inside the reactor over a temperature range of 370-425°C. The experimental apparatus comprises the following main components: N_2 tank, humidifier, preheater, reactor, scrubber, and fume hood. 316 Stainless steel pipes are used to connect the parts. Nitrogen gas is passed through the pipes, and vapor is added to the flow in the humidifier. Both gases then pass through the preheater and reactor. After the reactor, nitrogen, product gas HCl , and H_2O are directed to pass through the NaOH solution in the scrubber for HCl to react and produce NaCl .

Safety Precautions

- Each student should use Personal Protective Equipment of a P-100 half-mask, latex hand gloves, safety boots, and lab coat while conducting the experiments.
- The research student must complete the Compressed Gas Safety training and Respirator Program.
- The safety manual should be read and understood by the research student.
- A sign of no entry is indicated on the door to inform other personnel and to prevent them from entering the research lab while experiments are underway.
- The intended hours of experimentation will also be noted. The experiment will only be conducted during regular working hours when the technologists are working in the adjoining laboratory.

- The emergency procedures and safety actions must be thoroughly understood.

In-built Safety Features

- The nitrogen tank will be arranged in the research lab by storing it up against the wall, tied with a cylinder bracket.
- A Cole Palmer single-stage regulator with 580 CGA Fitting is used.
- Flow rates of up to 10 Liters per minute are permitted.
- Connection pipes are $\frac{1}{4}$, $\frac{1}{2}$, and 1-inch sizes of Swagelok 316 series. Swagelok fittings are used to connect the pipes and fittings. Assembling guidelines will be followed, and a leak test will be conducted to ensure the system is fully sealed.
- Two pressure safety valves (Swagelok SS-R4M8F8-EP) are located before the humidifier and the reactor to eliminate unnecessary pressure accumulation inside the reactor.
- Two check valves (Swagelok SS-8C-1) are located before the pressure valves to ensure one-way fluid flow.
- For heating, the preheater and the reactor, a cylindrical heating element Omega CRFC-1512/120-C-A, will be used. The heating process is controlled by the temperature controller Digi Key DTB4848CRE-ND. No contact is required.
- Swagelok union fittings are utilized to facilitate the assembling and disassembling of the reactor bed from the reactor. This action will be performed only when the reactor is at room temperature and not during the experiment. The leak test will be performed for assembled parts of the reactor each time. The reactor bed will be scrubbed and cleaned before usage again.
- The scrubber is fabricated from an acrylic plastic cylinder and flat plate glued with ABS cement. The sample from the NaOH solution is taken by the digital pipette Eppendorf Research(R) Plus Pipette.
- The chlorine gas meter and Forensics detectors FD-90A-CL2 (Range – 0-50ppm with 0.1 ppm resolution and response time less than 30 seconds) are used to ensure no chlorine is present within the lab.
- EDS-safe approved mobile fume extractor ZEROSMOGELKIT1N from Digi Key with a maximum flow rate of 220 cubic feet per minute, HEPA H13 particle filter, MS medium dust filter, and granular activated carbon filter will be utilized as a secondary safety measure.

Emergency Shutdown Procedures

- In case of an emergency, the following steps will be taken.
- Power to the humidifier, water bath, preheater, and reactor will be cut.
- The nitrogen tank will be disconnected from the regulator, and the experiment will be moved if necessary for operations such as cooling down.
- A fire extinguisher will be used if any fire breaks out.
- The lab technician will be informed.
- Possible causes of an emergency shutdown are listed below.
- The mobile fume extractor ceases to work.
- The chlorine sensor shows that chlorine is present in the atmosphere.
- The temperature inside the preheater and reactor exceeds the intended value, and the temperature controller seems to stop or malfunction.
- Any visual or audible leaks occur.
- The pressure safety valve begins to function.
- Any disassembling of a fitting or breaking a pipe has occurred during the experiment.
- An unusual appearance of the experiment such as a color change of steel pipes occurs due to high heat and vibrating.
- Any inline measuring unit fails to collect data.
- An electricity cut occurs.
- Please note that there might be other causes that are not listed above. Please experiment with care. Always be prepared for any unexpected circumstances.

Checklist

1. To conduct a safe experiment, the following steps will be taken each run.
2. The lab technician must be informed that the experiment is in progress.

3. Set the label “No entry- Experiment in progress” on the door.
4. Switch on the exhaust fan of the lab, which is connected to the wall.
5. Check the chlorine sensor and fume extractor function.
6. Wear the correct safety attire.
7. Measure the molarity of the NaOH solution.
8. Power the DAQ system and measuring equipment.
9. Let nitrogen pass through the pipes. Initially, there will be a spike in the flow rate from the flow control valve. Therefore, first, supply a flow rate (around 6SCCM) before connecting the reactor bed to the pipe system. Ensure the humidifier is bypassed.
10. Perform a soap leak test before starting the experiment using a Swagelok Snoop solution.
11. Keep the N₂ flow rate until the humidity sensor reading reaches zero to achieve a complete vapor-free flow rate.
12. Deionized water is poured into the humidifier pipe inside through the ball valve. This action will be performed only if the water bath is at room temperature and not during the experiment.
13. Check for any failed measuring items and ensure the function of the DAQ system.
14. Stop the nitrogen flow.
15. Insert a new mesh on the reactor bed. Thereafter apply CuCl₂.
16. Apply white taps on the threads on both ends to ease air tightening.
17. Assemble the reactor bed for the experiment.
18. From this step, neither power should be cut off, nor any change to the electrical circuit should be made.
19. Let nitrogen pass through the pipes again. The flow rate must not exceed 2 SCCM as it might displace the CuCl₂ powder on the reactor bed.
20. Check for leakages by performing a soap leak test with the Swagelok Snoop solution. Focus on newly connected parts.
21. Switch on the temperature controllers. Set the required temperatures for both temperature controllers to a value less than the room temperature to ensure that there will be no current passing to heaters.

22. Connect the preheater and reactor. Check for any visible and audible failures.
23. Increase the required temperatures of temperature controllers to desired values.
24. Start storing data from the DAQ system.
25. Check the measurements and wait until the required temperature appears.
26. From this step, desired results will be taken.
27. Start the fume extractor.
28. Adjust the three-way valve control for nitrogen to direct flow through the humidifier. Start the timer.
29. Samples will be collected at regular intervals from the scrubber solution.
30. From this point, the experiment is performed.
31. After the experiment is complete, use the three-way valve to change the nitrogen flow to the humidifier water bypassing line.
32. Power off the heaters and let the temperature inside the reactor cool down to room temperature.
33. Save the data file and power off the DAQ system.
34. Thereafter, stop nitrogen flow from the nitrogen tank. Wait until both gauges in the regulator become zero.
35. Set the nitrogen flow to zero.
36. Check all the electrical units are switched off and their plugs are disconnected from the grid.
37. Switch off the chlorine sensor, and fume extractor finally.
38. Keep the samples in a safe place. clean up the room.
39. Turn off the exhaust fan.
40. Remove the sign from the door.
41. Remove safety attire and dispose of items if they cannot be used further safely.
42. Disassemble the reactor bed and remove the mesh with reactants and products after cooling down.
This might take a day.
43. Insert a new mesh into the reactor bed. Clean the reactor bed.